# 3
# The Restricted Three-Body Problem

Two's company, three's a crowd.

Proverb

## 3.1 Introduction

In Chapter 2 we showed how the problem of the motion of two masses moving under their mutual gravitational attraction can be solved analytically and that the resulting motion is always confined to fixed geometrical paths that are closed in inertial space. We will now extend our analysis to consider the gravitational interaction of three bodies, paying particular attention to the problem in which the third body has negligible mass compared with the other two.

The simplicity and elusiveness of the three-body problem in its various forms have attracted the attention of mathematicians for centuries. Among the giants of mathematics who have tackled the problem and made important contributions are Euler, Lagrange, Laplace, Jacobi, Le Verrier, Hamilton, Poincaré, and Birkhoff. The books by Szebehely (1967) and Marchal (1990) provide authoritative coverage of the literature on the subject as well as derivations of the important results. Today the three-body problem is as enigmatic as ever and although much has been discovered already, the recent developments in nonlinear dynamics and the spur of new observations in the solar system have meant a resurgence of interest in the problem and the derivation of new results.

If two of the bodies in the problem move in circular, coplanar orbits about their common centre of mass and the mass of the third body is too small to affect the motion of the other two bodies, the problem of the motion of the third body is called the *circular, restricted, three-body problem*. At first glance this problem may seem to have little application to motion in the solar system. After all, the observed orbits of solar system objects are noncoplanar and noncircular. However, the hierarchy of orbits and masses in the solar system (e.g., Sun, planet, satellite, ring particle) means that the restricted three-body problem provides a

good approximation for certain systems and that the qualitative behaviour of the motion can be understood by relatively simple analysis. In this context we will study systems that have applications to typical problems in the solar system, thereby excluding the more exotic variations of the three-body problem, such as the Copenhagen problem (where the two large masses are equal), the Pythagorean problem (where the three bodies have initial masses in the ratio 3:4:5 and initial positions on a 3,4,5 right-angled triangle), and triple collisions (where the three bodies can "pass through" one another).

In this chapter we describe the equations of motion of the three-body problem and discuss the location and stability of equilibrium points with particular reference to a constant of the motion, the Jacobi integral, in the circular restricted case. We demonstrate the relationship between curves defined by the Jacobi integral and the orbital path of the particle. We derive Hill's equations to study the motion of the particle in the vicinity of one of the masses and show the general properties of such a system. Finally, we discuss the effects of drag forces in the three-body problem.

## 3.2 Equations of Motion

We consider the motion of a small particle of negligible mass moving under the gravitational influence of two masses $m_1$ and $m_2$. We assume that the two masses have circular orbits about their common centre of mass and that they exert a force on the particle although the particle cannot affect the two masses.

Consider a set of axes $\xi$, $\eta$, $\zeta$ in the inertial frame referred to the centre of mass of the system (see Fig. 3.1). Let the $\xi$ axis lie along the line from $m_1$ to $m_2$ at time $t = 0$ with the $\eta$ axis perpendicular to it and in the orbital plane of the two masses and the $\zeta$ axis perpendicular to the $\xi$–$\eta$ plane, along the angular momentum vector. Let the coordinates of the two masses in this reference frame be $(\xi_1, \eta_1, \zeta_1)$ and $(\xi_2, \eta_2, \zeta_2)$. The two masses have a constant separation and the same angular velocity about each other and their common centre of mass. Let the unit of mass be chosen such that $\mu = \mathcal{G}(m_1 + m_2) = 1$. If we now assume that $m_1 > m_2$ and define

$$\bar{\mu} = \frac{m_2}{m_1 + m_2} \tag{3.1}$$

then in this system of units the two masses are

$$\mu_1 = \mathcal{G}m_1 = 1 - \bar{\mu} \qquad \text{and} \qquad \mu_2 = \mathcal{G}m_2 = \bar{\mu}, \tag{3.2}$$

where $\bar{\mu} < 1/2$. The unit of length is chosen such that the constant separation of the two masses is unity. It then follows that the common mean motion, $n$, of the two masses is also unity.

Let the coordinates of the particle in the *inertial*, or *sidereal*, *system*, be $(\xi, \eta, \zeta)$. By applying the vector form of the inverse square law, the equations of

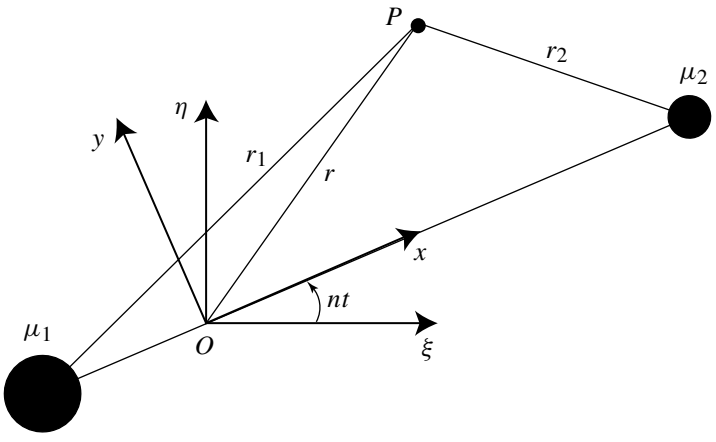


Fig. 3.1. A planar view of the relationship between the sidereal coordinates $(\xi, \eta, \zeta)$ and the synodic coordinates $(x, y, z)$ of the particle at the point $P$. The origin $O$ is located at the centre of mass of the two bodies. The $\zeta$ and $z$ axes coincide with the axis of rotation and the arrow indicates the direction of positive rotation.

motion of the particle are

$$\ddot{\xi} = \mu_1 \frac{\xi_1 - \xi}{r_1^3} + \mu_2 \frac{\xi_2 - \xi}{r_2^3}, \tag{3.3}$$

$$\ddot{\eta} = \mu_1 \frac{\eta_1 - \eta}{r_1^3} + \mu_2 \frac{\eta_2 - \eta}{r_2^3}, \tag{3.4}$$

$$\ddot{\zeta} = \mu_1 \frac{\zeta_1 - \zeta}{r_1^3} + \mu_2 \frac{\zeta_2 - \zeta}{r_2^3}, \tag{3.5}$$

where, from Fig. 3.1,

$$r_1^2 = (\xi_1 - \xi)^2 + (\eta_1 - \eta)^2 + (\zeta_1 - \zeta)^2, \tag{3.6}$$

$$r_2^2 = (\xi_2 - \xi)^2 + (\eta_2 - \eta)^2 + (\zeta_1 - \zeta)^2. \tag{3.7}$$

Note that these equations are also valid in the general three-body problem since they do not require any assumptions about the paths of the two masses.

If the two masses are moving in circular orbits then the distance between them is fixed and they move about their common centre of mass at a fixed angular velocity, the mean motion $n$. In these circumstances it is natural to consider the motion of the particle in a rotating reference frame in which the locations of the two masses are also fixed. Consider a new, rotating coordinate system that has the same origin as the $\xi, \eta$ system but which is rotating at a uniform rate $n$ in the positive direction (see Fig. 3.1). The direction of the $x$ axis is chosen such that the two masses always lie along it with coordinates $(x_1, y_1, z_1) = (-\mu_2, 0, 0)$ and

$(x_2, y_2, z_2) = (\mu_1, 0, 0)$. Hence, from Eq. (3.2) and Fig. 3.1 we have

$$r_1^2 = (x + \mu_2)^2 + y^2 + z^2, \tag{3.8}$$
$$r_2^2 = (x - \mu_1)^2 + y^2 + z^2, \tag{3.9}$$

where $(x, y, z)$ are the coordinates of the particle with respect to the rotating, or *synodic*, *system*. These coordinates are related to the coordinates in the sidereal system by the simple rotation

$$\begin{pmatrix} \xi \\ \eta \\ \zeta \end{pmatrix} = \begin{pmatrix} \cos nt & -\sin nt & 0 \\ \sin nt & \cos nt & 0 \\ 0 & 0 & 1 \end{pmatrix} \begin{pmatrix} x \\ y \\ z \end{pmatrix}. \tag{3.10}$$

Although in our system of units $n = 1$, we will retain $n$ in the equations to emphasise that all the terms in the equations of motion are accelerations.

If we now differentiate each component in Eq. (3.10) twice we obtain

$$\begin{pmatrix} \dot{\xi} \\ \dot{\eta} \\ \dot{\zeta} \end{pmatrix} = \begin{pmatrix} \cos nt & -\sin nt & 0 \\ \sin nt & \cos nt & 0 \\ 0 & 0 & 1 \end{pmatrix} \begin{pmatrix} \dot{x} - ny \\ \dot{y} + nx \\ \dot{z} \end{pmatrix} \tag{3.11}$$

and

$$\begin{pmatrix} \ddot{\xi} \\ \ddot{\eta} \\ \ddot{\zeta} \end{pmatrix} = \begin{pmatrix} \cos nt & -\sin nt & 0 \\ \sin nt & \cos nt & 0 \\ 0 & 0 & 1 \end{pmatrix} \begin{pmatrix} \ddot{x} - 2n\dot{y} - n^2 x \\ \ddot{y} + 2n\dot{x} - n^2 y \\ \ddot{z} \end{pmatrix}. \tag{3.12}$$

Note that the switch to a rotating reference frame has introduced terms in $n\dot{x}$ and $n\dot{y}$ (the *Corioli's acceleration*) and $n^2 x$ and $n^2 y$ (the *centrifugal acceleration*) into the equations of motion. Using these substitutions for $\xi$, $\eta$, $\zeta$, $\ddot{\xi}$, $\ddot{\eta}$, and $\ddot{\zeta}$, Eqs. (3.3), (3.4), and (3.5) become

$$(\ddot{x} - 2n\dot{y} - n^2 x)\cos nt - (\ddot{y} + 2n\dot{x} - n^2 y)\sin nt = \left[\mu_1 \frac{x_1 - x}{r_1^3} + \mu_2 \frac{x_2 - x}{r_2^3}\right]\cos nt + \left[\frac{\mu_1}{r_1^3} + \frac{\mu_2}{r_2^3}\right] y \sin nt, \tag{3.13}$$

$$(\ddot{x} - 2n\dot{y} - n^2 x)\sin nt + (\ddot{y} + 2n\dot{x} - n^2 y)\cos nt = \left[\mu_1 \frac{x_1 - x}{r_1^3} + \mu_2 \frac{x_2 - x}{r_2^3}\right]\sin nt - \left[\frac{\mu_1}{r_1^3} + \frac{\mu_2}{r_2^3}\right] y \cos nt, \tag{3.14}$$

$$\ddot{z} = -\left[\frac{\mu_1}{r_1^3} + \frac{\mu_2}{r_2^3}\right] z. \tag{3.15}$$

If we multiply Eq. (3.13) by $\cos nt$, and Eq. (3.14) by $\sin nt$, and add the results, and then multiply Eq. (3.13) by $-\sin nt$, and Eq. (3.14) by $\cos nt$, and add these

together, the equations of motion in the synodic system become

$$\ddot{x} - 2n\dot{y} - n^2 x = -\left[\mu_1 \frac{x+\mu_2}{r_1^3} + \mu_2 \frac{x-\mu_1}{r_2^3}\right], \tag{3.16}$$

$$\ddot{y} + 2n\dot{x} - n^2 y = -\left[\frac{\mu_1}{r_1^3} + \frac{\mu_2}{r_2^3}\right] y, \tag{3.17}$$

$$\ddot{z} = -\left[\frac{\mu_1}{r_1^3} + \frac{\mu_2}{r_2^3}\right] z. \tag{3.18}$$

These accelerations can also be written as the gradient of a scalar function $U$:

$$\ddot{x} - 2n\dot{y} = \frac{\partial U}{\partial x}, \tag{3.19}$$

$$\ddot{y} + 2n\dot{x} = \frac{\partial U}{\partial y}, \tag{3.20}$$

$$\ddot{z} = \frac{\partial U}{\partial z}, \tag{3.21}$$

where $U = U(x, y, z)$ is given by

$$U = \frac{n^2}{2}(x^2 + y^2) + \frac{\mu_1}{r_1} + \frac{\mu_2}{r_2}. \tag{3.22}$$

In this equation the term in $x^2 + y^2$ is the centrifugal potential and the term in $1/r_2$ and $1/r_2$ is the gravitational potential, the partial derivatives of which give rise to the centrifugal and gravitational forces, respectively.

The $-2n\dot{y}$ and $+2n\dot{x}$ terms in Eqs. (3.19) and (3.20) are the Corioli's terms, which depend on the velocity of the particle in the rotating reference frame. The resulting Corioli's force is at right angles to the velocity and therefore does no work.

Note that in our definition $U$ is positive. However, this is opposite to the practice in physics and is purely a convention in celestial mechanics. We could equally well have taken it to be negative, say $U^* = -U$, and the equations of motion would become

$$\ddot{x} - 2n\dot{y} = -\frac{\partial U^*}{\partial x}, \tag{3.23}$$

$$\ddot{y} + 2n\dot{x} = -\frac{\partial U^*}{\partial y}, \tag{3.24}$$

$$\ddot{z} = -\frac{\partial U^*}{\partial z}. \tag{3.25}$$

Note also that $U$ is not a true potential and it is best referred to as a scalar function from which some (but not all) of the accelerations experienced by the particle in the rotating frame can be derived. $U$ is called a "pseudo-potential."

### 3.3 The Jacobi Integral

Multiplying Eq. (3.19) by $\dot{x}$, and Eq. (3.20) by $\dot{y}$, and Eq. (3.21) by $\dot{z}$ and adding we have

$$\dot{x}\ddot{x} + \dot{y}\ddot{y} + \dot{z}\ddot{z} = \frac{\partial U}{\partial x}\dot{x} + \frac{\partial U}{\partial y}\dot{y} + \frac{\partial U}{\partial z}\dot{z} = \frac{\mathrm{d}U}{\mathrm{d}t}. \tag{3.26}$$

This can be integrated to give

$$\dot{x}^2 + \dot{y}^2 + \dot{z}^2 = 2U - C_\mathrm{J}, \tag{3.27}$$

where $C_\mathrm{J}$ is a constant of integration. Since $\dot{x}^2 + \dot{y}^2 + \dot{z}^2 = v^2$, the square of the velocity of the particle in the rotating frame, we have

$$v^2 = 2U - C_\mathrm{J} \tag{3.28}$$

or, using Eq. (3.22),

$$C_\mathrm{J} = n^2(x^2 + y^2) + 2\left(\frac{\mu_1}{r_1} + \frac{\mu_2}{r_2}\right) - \dot{x}^2 - \dot{y}^2 - \dot{z}^2. \tag{3.29}$$

This demonstrates that the quantity $2U - v^2 = C_\mathrm{J}$ is a constant of the motion. This is the *Jacobi integral*, or Jacobi constant, sometimes called the *integral of relative energy.* It is important to note that this is not an energy integral because in the restricted problem neither energy nor angular momentum is conserved. The Jacobi integral is the only integral of the circular restricted three-body problem and this means that the problem cannot be solved in closed form for general cases.

The expression for $C_\mathrm{J}$ can also be written in terms of the position and velocity of the particle in the nonrotating, sidereal frame. For the position vectors we can use Eq. (3.10) to obtain

$$\begin{pmatrix} x \\ y \\ z \end{pmatrix} = \begin{pmatrix} \cos nt & \sin nt & 0 \\ -\sin nt & \cos nt & 0 \\ 0 & 0 & 1 \end{pmatrix} \begin{pmatrix} \xi \\ \eta \\ \zeta \end{pmatrix}. \tag{3.30}$$

For the velocity vectors we can use Eq. (3.11) to obtain

$$\begin{pmatrix} \dot{x} - ny \\ \dot{y} + nx \\ \dot{z} \end{pmatrix} = \begin{pmatrix} \cos nt & \sin nt & 0 \\ -\sin nt & \cos nt & 0 \\ 0 & 0 & 1 \end{pmatrix} \begin{pmatrix} \dot{\xi} \\ \dot{\eta} \\ \dot{\zeta} \end{pmatrix}. \tag{3.31}$$

However,

$$\begin{pmatrix} \dot{x} - ny \\ \dot{y} + nx \\ \dot{z} \end{pmatrix} = \begin{pmatrix} \dot{x} \\ \dot{y} \\ \dot{z} \end{pmatrix} + n \begin{pmatrix} \sin nt & -\cos nt & 0 \\ \cos nt & \sin nt & 0 \\ 0 & 0 & 0 \end{pmatrix} \begin{pmatrix} \xi \\ \eta \\ \zeta \end{pmatrix} \tag{3.32}$$

and hence

$$\begin{pmatrix} \dot{x} \\ \dot{y} \\ \dot{z} \end{pmatrix} = \begin{pmatrix} \cos nt & \sin nt & 0 \\ -\sin nt & \cos nt & 0 \\ 0 & 0 & 1 \end{pmatrix} \begin{pmatrix} \dot{\xi} \\ \dot{\eta} \\ \dot{\zeta} \end{pmatrix} - n \begin{pmatrix} \sin nt & -\cos nt & 0 \\ \cos nt & \sin nt & 0 \\ 0 & 0 & 0 \end{pmatrix} \begin{pmatrix} \xi \\ \eta \\ \zeta \end{pmatrix}. \tag{3.33}$$

If we let

$$\mathbf{A} = \begin{pmatrix} \cos nt & \sin nt & 0 \\ -\sin nt & \cos nt & 0 \\ 0 & 0 & 1 \end{pmatrix} \quad \text{and} \quad \mathbf{B} = \begin{pmatrix} \sin nt & -\cos nt & 0 \\ \cos nt & \sin nt & 0 \\ 0 & 0 & 0 \end{pmatrix} \tag{3.34}$$

then, from Eq. (3.33),

$$\begin{aligned} \dot{x}^2 + \dot{y}^2 + \dot{z}^2 &= (\dot{x} \quad \dot{y} \quad \dot{z}) \begin{pmatrix} \dot{x} \\ \dot{y} \\ \dot{z} \end{pmatrix} \\ &= (\dot{\xi} \quad \dot{\eta} \quad \dot{\zeta})\, \mathbf{A}^{\mathrm{T}}\mathbf{A} \begin{pmatrix} \dot{\xi} \\ \dot{\eta} \\ \dot{\zeta} \end{pmatrix} - n\,(\dot{\xi} \quad \dot{\eta} \quad \dot{\zeta})\, \mathbf{A}^{\mathrm{T}}\mathbf{B} \begin{pmatrix} \xi \\ \eta \\ \zeta \end{pmatrix} \\ &\quad - n\,(\xi \quad \eta \quad \zeta)\, \mathbf{B}^{\mathrm{T}}\mathbf{A} \begin{pmatrix} \dot{\xi} \\ \dot{\eta} \\ \dot{\zeta} \end{pmatrix} + n^2\,(\xi \quad \eta \quad \zeta)\, \mathbf{B}^{\mathrm{T}}\mathbf{B} \begin{pmatrix} \xi \\ \eta \\ \zeta \end{pmatrix} \\ &= \dot{\xi}^2 + \dot{\eta}^2 + \dot{\zeta}^2 + n^2(\xi^2 + \eta^2) + 2n(\dot{\xi}\eta - \dot{\eta}\xi), \end{aligned} \tag{3.35}$$

where $\mathbf{A}^{\mathrm{T}}$ and $\mathbf{B}^{\mathrm{T}}$ denote the transposes of the matrices $\mathbf{A}$ and $\mathbf{B}$. Since $\mathbf{A}$ and $\mathbf{B}$ are both orthogonal matrices, their inverses are simply their transposes. Because distances are always unchanged by rotations (or, equivalently, since the determinants of orthogonal matrices are equal to unity) we also have $x^2+y^2+z^2 = \xi^2 + \eta^2 + \zeta^2$; this can also be obtained from Eq. (3.10). We obtain

$$C_{\mathrm{J}} = 2\left(\frac{\mu_1}{r_1} + \frac{\mu_2}{r_2}\right) + 2n(\xi\dot{\eta} - \eta\dot{\xi}) - \dot{\xi}^2 - \dot{\eta}^2 - \dot{\zeta}^2 \tag{3.36}$$

for the expression for the Jacobi constant in terms of the sidereal coordinates. We can rewrite this as

$$\frac{1}{2}\left(\dot{\xi}^2 + \dot{\eta}^2 + \dot{\zeta}^2\right) - \left(\frac{\mu_1}{r_1} + \frac{\mu_2}{r_2}\right) = \mathbf{h} \cdot \mathbf{n} - \frac{1}{2}C_{\mathrm{J}}, \tag{3.37}$$

where $\mathbf{n} = (0, 0, n)$ and the left-hand side of the equation is the total, or mechanical, energy per unit mass of the particle. Because $\mathbf{h} \cdot \mathbf{n}$ is not a constant, this explains why energy is not conserved in the restricted three-body problem.

The measurement of the particle's position and velocity in either frame determines the value of the Jacobi constant associated with the motion of the particle. The existence of the angular momentum and energy integrals in the two-body problem enabled us to solve for the motion of one mass with respect to the other (see Sect. 2.3). The Jacobi constant is the only integral of the motion in the

restricted three-body problem. We cannot make use of it to provide an exact solution for the orbital motion, but we can use it to determine regions from which the particle is excluded.

The usefulness of the Jacobi constant can be appreciated by considering the locations where the velocity of the particle is zero. In this case we have

$$2U = C_{\mathrm{J}} \tag{3.38}$$

or

$$n^2(x^2 + y^2) + 2\left(\frac{\mu_1}{r_1} + \frac{\mu_2}{r_2}\right) = C_{\mathrm{J}}. \tag{3.39}$$

Equation (3.39) defines a set of surfaces for particular values of $C_{\mathrm{J}}$. These surfaces, known as the *zero-velocity surfaces*, play an important role in placing bounds on the motion of the particle. For simplicity we restrict ourselves to the $x$–$y$ plane. In this case the intersection of the zero-velocity surfaces with the $x$–$y$ plane produces a set of *zero-velocity curves*. Figure 3.2 shows examples of these curves for the case $\mu_2 = 0.2$; the mean motion $n$ is taken to be unity. From our expression for the Jacobi constant, Eq. (3.27), it is clear that we must always have $2U \geq C_{\mathrm{J}}$ since otherwise the velocity $v$ would be complex. Thus Eq. (3.39) defines the boundary curves of regions where particle motion is not possible, in other words excluded regions. Hence, although the restricted three-body problem is not integrable (we cannot solve for the motion of the particle for arbitrary starting conditions), the existence of the Jacobi integral does permit us to find regions of $x$–$y$ space where the particle cannot be. The result is easily extended to three dimensions.

Since the shaded areas in Fig. 3.2 denote regions where motion is impossible, we can see from Fig. 3.2a, for example, that if a particle with that value of $C_{\mathrm{J}}$ is in orbit in the unshaded region around the mass $\mu_1$ then it can never orbit the mass $\mu_2$ or escape from the system since it would have to cross the excluded region to

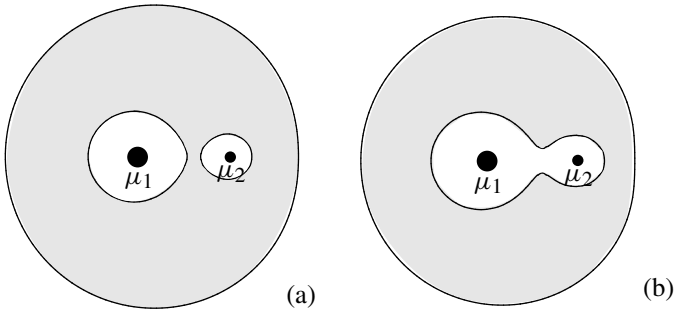


Fig. 3.2. Zero-velocity curves for two values of the Jacobi constant for the case when $\mu_2 = 0.2$. The values of $C_{\mathrm{J}}$ are (a) $C_{\mathrm{J}} = 3.9$, (b) $C_{\mathrm{J}} = 3.7$. The shaded areas denote the excluded regions. (See also Fig. 9.11 for the case $\mu_2 = 10^{-3}$.)

do so. Similarly, in Fig. 3.2b, if the particle is originally orbiting the mass $\mu_1$ then it is possible that it could eventually orbit the mass $\mu_2$, but it could never escape from the system. This is the concept of *Hill's stability*. However, it is useful to recall that such statements are only valid under the assumptions inherent in the restricted three-body problem (i.e., the two masses move in circular orbits about their common centre of mass, and the third mass has no gravitational influence on the other two).

## 3.4 The Tisserand Relation

Consider a comet with initial semi-major axis $a$, eccentricity $e$, and inclination $I$. Following a close approach to Jupiter the comet's orbital elements become $a'$, $e'$, and $I'$. We can use the Jacobi integral and some simple approximations to relate these two sets of elements. The Jacobi integral, given by $C_\mathrm{J} = 2U - v^2$, remains constant throughout the encounter. In three-dimensional, inertial space the comet has a position vector $\mathbf{r} = (\xi, \eta, \zeta)$ and velocity vector $\dot{\mathbf{r}} = (\dot{\xi}, \dot{\eta}, \dot{\zeta})$. In this system we can use Eq. (3.37) to write the Jacobi constant as

$$C_\mathrm{J} = 2\left(\frac{\mu_1}{r_1} + \frac{\mu_2}{r_2}\right) + 2n(\xi\dot{\eta} - \eta\dot{\xi}) - \dot{\xi}^2 - \dot{\eta}^2 - \dot{\zeta}^2, \tag{3.40}$$

where $r_1$ and $r_2$ are the distances of the comet from the Sun and Jupiter respectively. We will also choose units such that the semi-major axis and mean motion of Jupiter's orbit are unity and, since the mass of Jupiter and the comet are much smaller than the Sun's mass,

$$\mathcal{G}\left(m_\mathrm{Sun} + m_\mathrm{comet}\right) \approx \mathcal{G}\left(m_\mathrm{Sun} + m_\mathrm{Jupiter}\right) = 1, \tag{3.41}$$

where $m_\mathrm{Sun}$, $m_\mathrm{Jupiter}$, and $m_\mathrm{comet}$ are the masses of the Sun, Jupiter, and the comet respectively. From the energy integral of the Sun–comet two-body problem (see Eq. (2.34)) we have

$$\dot{\xi}^2 + \dot{\eta}^2 + \dot{\zeta}^2 = \frac{2}{r} - \frac{1}{a}, \tag{3.42}$$

where we have taken $\mu = 1$ in accordance with our system of units and where we are assuming $r_1 \approx r$ since the mass of the comet and Jupiter are effectively negligible compared with the mass of the Sun. The angular momentum per unit mass of the comet's orbit is given by

$$\mathbf{h} = \mathbf{r} \times \dot{\mathbf{r}}. \tag{3.43}$$

If $I$ is the inclination of the comet's orbit relative to the plane of Jupiter's orbit, then the $\zeta$ component of the angular momentum vector is given by

$$\xi\dot{\eta} - \eta\dot{\xi} = h\cos I, \tag{3.44}$$

where $h^2 = a(1 - e^2)$ in our system of units. Therefore the form of the Jacobi integral expressed in Eq. (3.40) implies

$$\frac{2}{r} - \frac{1}{a} - 2\sqrt{a(1-e^2)}\cos I = \frac{2}{r} - 2\mu_2\left(\frac{1}{r} - \frac{1}{r_2}\right) - C_{\mathrm{J}}. \tag{3.45}$$

If we assume that the comet is not close to Jupiter so that $1/r_2$ is always a small quantity and neglect the $\mu_2$ terms, we have

$$\frac{1}{2a} + \sqrt{a(1-e^2)}\cos I \approx \text{constant}. \tag{3.46}$$

Therefore the approximate relationship between the orbital elements of the comet before and after the encounter with Jupiter is given by

$$\frac{1}{2a} + \sqrt{a(1-e^2)}\cos I = \frac{1}{2a'} + \sqrt{a'(1-e'^2)}\cos I'. \tag{3.47}$$

This is known as the *Tisserand relation* (Tisserand 1896) and it can be used to determine whether or not a newly discovered comet is a previously known object that has had its orbital elements changed by a close approach to a planet.

An example of such an encounter for a hypothetical comet is shown in Fig. 3.3. A close approach to Jupiter alters the orbital elements of the comet with the semi-major axis increasing by almost 8 AU. The initial orbital elements of the comet

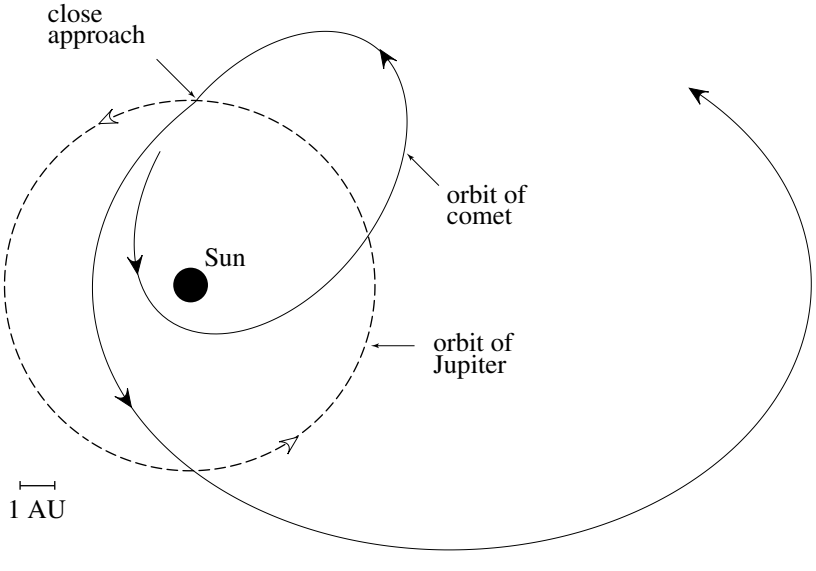


Fig. 3.3. The changing orbit of a hypothetical comet that has a close approach to Jupiter. The encounter produces large changes in the orbital elements of the comet.

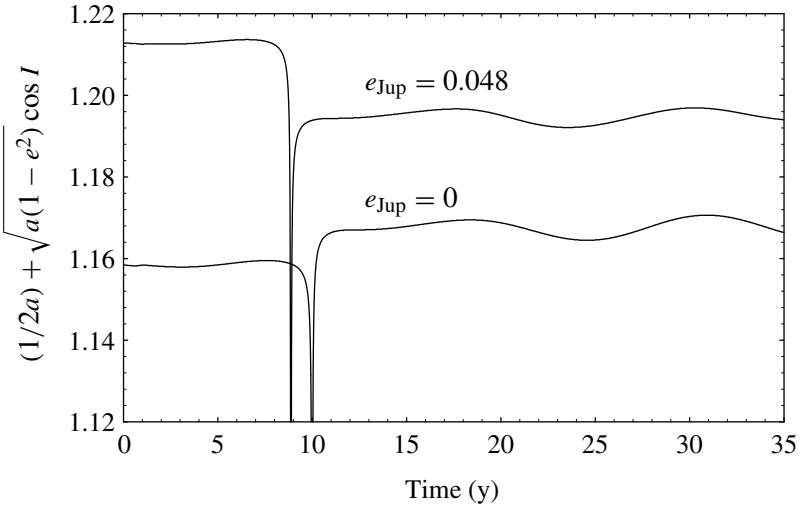


Fig. 3.4. The variation of the Tisserand constant throughout the 35 y integration of the two cometary orbits for the cases where $e_{\rm Jup} = 0$ and $e_{\rm Jup} = 0.048$.

are $a = 4.81$ AU ($= 0.924$ in our units), $e = 0.763$, and $I = 7\overset{\circ}{.}47$ while the final elements are $a' = 10.8$ AU, $e' = 0.731$, and $I' = 21\overset{\circ}{.}4$.

Although the Tisserand relation is only an approximation to the Jacobi constant and is derived by assuming that Jupiter is in a circular orbit, the quantity $(1/2a) + \sqrt{a(1-e^2)}\cos I$ is still an approximate constant of the motion in the case where the eccentricity of Jupiter is nonzero. This is illustrated in Fig. 3.4 where the variation in this quantity is plotted as a function of time for two separate numerical integrations. In the first case (the lower curve) Jupiter is taken to move in a circular orbit, while in the second case the eccentricity of Jupiter is taken to have its current value of 0.048. Apart from a short time interval near closest approach where the approximation is invalid, the value of the Tisserand constant changes by less than 1% in the former case and less than 2% in the latter. The regular variations away from closest approach have a period equal to Jupiter's period of 12 y.

The difference in the orbit of the comet before and after its close approach to Jupiter shown in Fig. 3.3 illustrates the dramatic effects of planetary encounters. The same technique is used to obtain gravitational assists for spacecraft such as *Voyager*, *Galileo*, and *Cassini* journeying to the outer planets of the solar system. The above analysis is based on the circular restricted problem where the mass of the third body (the comet or spacecraft) is negligible and hence there is no conservation of energy. However, in the actual situation there is energy conservation and a close approach that increases the semi-major axis of the third body will result in a decay of the semi-major axis of the perturbing body. Because the spacecraft to planet mass ratio is so small, the effect on the planet is

undetectable. However, in the early solar system close encounters between the major planets and planetesimals resulted in the formation of the Oort cloud of comets and the cumulative effects of these close encounters on the orbits of the planets were probably large (Fernandez 1997).

## 3.5 Lagrangian Equilibrium Points

We have shown that in the case where the two masses $m_1$ and $m_2$ move in circular orbits about their common centre of mass, $O$, their positions are stationary in a frame rotating with an angular velocity equal to the mean motion $n$ of either mass. We will approach the subject of *equilibrium points* by considering the problem of finding the location of the points where a particle $P$ could be placed, with the appropriate velocity in the inertial frame, where it remains stationary in the rotating frame. It is important to remember that at such an equilibrium position the particle is still subject to a number of forces and that it is still moving in a keplerian orbit in the inertial frame.

Let **a**, **b**, and **c** denote the location of the mass $m_1$, the centre of mass, $O$, and the mass $m_2$ with respect to the point $P$ (see Fig. 3.5). Let $\mathbf{F}_1$ and $\mathbf{F}_2$ denote the forces per unit mass on the particle directed towards the masses $m_1$ and $m_2$ respectively. For $P$ to be at a fixed location in the rotating frame, it must be at a fixed distance $b$ from $O$, which is the only fixed point in the inertial frame. Therefore $P$ is subject to a centrifugal acceleration in the $-\mathbf{b}$ direction and this is balanced by the vector sum

$$\mathbf{F} = \mathbf{F}_1 + \mathbf{F}_2, \tag{3.48}$$

which lies in the direction of **b** and passes through the centre of mass. Note that here we do not need to take the Coriolis force into account because the particle is stationary in the rotating frame.

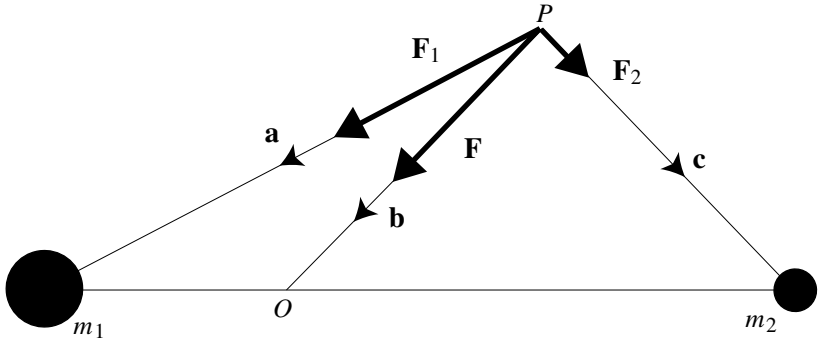


Fig. 3.5. The forces experienced by a test particle $P$ due to the gravitational attraction of the two masses $m_1$ and $m_2$. The point $O$ denotes the location of the centre of mass of $m_1$ and $m_2$.

The position of $O$ is given by

$$\mathbf{b} = \frac{m_1\mathbf{a} + m_2\mathbf{c}}{m_1 + m_2} \tag{3.49}$$

or, rearranging,

$$m_1(\mathbf{a} - \mathbf{b}) = m_2(\mathbf{b} - \mathbf{c}). \tag{3.50}$$

Taking the vector product of $\mathbf{F}_1 + \mathbf{F}_2$ with Eq. (3.50) gives

$$m_2(\mathbf{F}_1 \times \mathbf{c}) + m_1(\mathbf{F}_2 \times \mathbf{a}) = \mathbf{0}\,. \tag{3.51}$$

Since the angle between $\mathbf{F}_1$ and $\mathbf{c}$ is minus the angle between $\mathbf{F}_2$ and $\mathbf{a}$, we can write the scalar form of Eq. (3.51) as

$$m_2F_1c = m_1F_2a\,. \tag{3.52}$$

In the case of gravitational forces, $F_1 = \mathcal{G}m_1/a^2$ and $F_2 = \mathcal{G}m_2/c^2$ and hence, from Eq. (3.52), $a = c$. Therefore the triangle formed by joining the particle to the two masses must be an isosceles triangle. This implies that the locus of all points $P$ for which $\mathbf{F}$ passes through the centre of mass is the perpendicular bisector of the line joining $m_1$ and $m_2$ (the dashed line in Fig. 3.6).

To balance the centrifugal acceleration of $P$ with the force per unit mass directed towards the centre of mass, we must have

$$n^2b = F_1\cos\beta + F_2\cos\gamma, \tag{3.53}$$

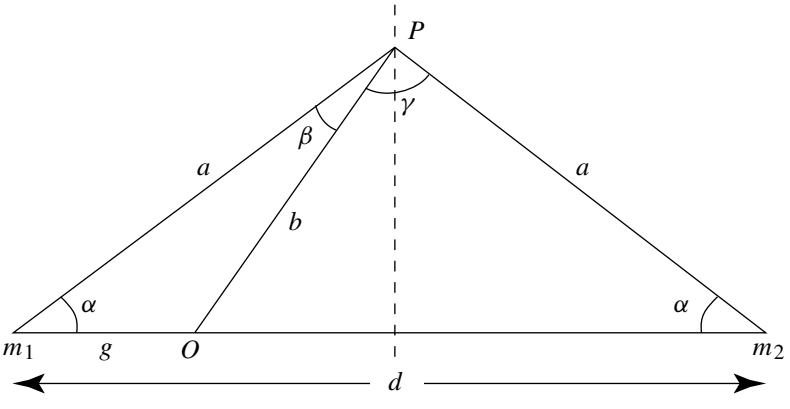


Fig. 3.6. The geometry of the balance of forces where $P$ denotes the location of a test particle at an equilibrium position. The dashed line denotes the perpendicular bisector of the line joining the two masses, $m_1$ and $m_2$; this is the locus of equilibrium positions in the case of gravitational forces.

where $\beta$ is the angle between $\mathbf{F}_1$ and $\mathbf{b}$, and $\gamma$ is the angle between $\mathbf{F}_2$ and $\mathbf{b}$ (see Fig. 3.6). Therefore

$$n^2 = \frac{\mathcal{G}}{a^2 b^2}(m_1 b\cos\beta + m_2 b\cos\gamma)\,. \tag{3.54}$$

However, by inspection of the triangles formed by $O$, $P$, and the two masses, we have

$$\begin{aligned} b\cos\beta &= a - g\cos\alpha,\\ b\cos\gamma &= a - (d-g)\cos\alpha, \end{aligned} \tag{3.55}$$

where $d$ is the distance between $m_1$ and $m_2$ and $g$ is the distance between $m_1$ and $O$, and

$$\cos\alpha = \frac{d}{2a}\,. \tag{3.56}$$

Furthermore, from the definition of the centre of mass, we have

$$\begin{aligned} g &= \frac{m_2}{m_1+m_2}d,\\ d-g &= \frac{m_1}{m_1+m_2}d. \end{aligned} \tag{3.57}$$

Thus Eq. (3.54) becomes

$$n^2 = \frac{\mathcal{G}(m_1+m_2)}{a^3 b^2}\left(a^2 - \frac{m_1 m_2}{(m_1+m_2)^2}d^2\right)\,. \tag{3.58}$$

From the cosine rule,

$$b^2 = a^2 + g^2 - 2ag\cos\alpha = a^2 + g^2 - gd\,. \tag{3.59}$$

Substituting in this equation the expression for $g$ from Eq. (3.57) and rearranging gives

$$b^2 = a^2 - \frac{m_1 m_2}{(m_1+m_2)^2}d^2, \tag{3.60}$$

and so Eq. (3.58) becomes

$$n^2 = \mathcal{G}(m_1+m_2)/a^3\,. \tag{3.61}$$

However, the reference frame is rotating in inertial space with an angular velocity $n$, where, from Eq. (2.22),

$$n^2 = \mathcal{G}(m_1+m_2)/d^3, \tag{3.62}$$

and hence we must have $a = d$. The same result can be derived by balancing the vector force in an arbitrary direction. If this direction is chosen to be normal to line joining $m_1$ and $m_2$ then the result follows immediately.

Therefore, in the case of the gravitational force exerted by $m_1$ and $m_2$, the system has an equilibrium point at the apex of an equilateral triangle with a base formed by the line joining the two masses. This result implies the existence of

another equilibrium point located below the same line, also lying at the apex of an equilateral triangle. These are the *Lagrangian equilibrium points* $L_4$ and $L_5$ respectively. In the classical problem there are three more equilibrium points, $L_1$, $L_2$, and $L_3$, which lie along the line joining the two masses.

Although we have only considered gravitational forces, it is important to realise that a similar analysis can be carried out for any time-independent force. For example, in the presence of drag forces the location of the shifted equilibrium points can be located using the fact that the resultant of all the forces must lie along a line pointing towards the centre of mass of the system. This is just another way of stating that the sum of all accelerations must be equal and opposite to the centrifugal acceleration in the rotating frame.

## 3.6 Location of Equilibrium Points

Although the circular restricted three-body problem is not integrable we can find a number of special solutions. This can be achieved by searching for points where the particle has zero velocity and zero acceleration in the rotating frame. Such points are called equilibrium points of the system (cf. Sect. 3.5). From now on we assume that all motion is confined to the $x$–$y$ plane. We also choose the unit of distance to be the constant separation of the two masses. It then follows that $n = 1$. None of these assumptions changes the essential dynamics of the system.

To facilitate the calculation of the locations of the equilibrium points we follow the example of Brouwer & Clemence (1961) and rewrite $U$ in a different form. From the definitions of $r_1$ and $r_2$ in Eqs. (3.8) and (3.9), and using the fact that $\mu_1 + \mu_2 = 1$, we have

$$\mu_1 r_1^2 + \mu_2 r_2^2 = x^2 + y^2 + \mu_1 \mu_2 \tag{3.63}$$

and hence

$$U = \mu_1 \left( \frac{1}{r_1} + \frac{r_1^2}{2} \right) + \mu_2 \left( \frac{1}{r_2} + \frac{r_2^2}{2} \right) - \frac{1}{2} \mu_1 \mu_2. \tag{3.64}$$

The advantage of this expression for $U$ is that the explicit dependence on $x$ and $y$ is removed, and so the partial derivatives become simpler. Note that $r_1$ and $r_2$, unlike $x$ and $y$, are always positive quantities.

Now consider the equations of motion, Eqs. (3.19) and (3.20), with $\ddot{x} = \ddot{y} = \dot{x} = \dot{y} = 0$. To find the locations of the equilibrium points we must solve the simultaneous nonlinear equations

$$\frac{\partial U}{\partial x} = \frac{\partial U}{\partial r_1} \frac{\partial r_1}{\partial x} + \frac{\partial U}{\partial r_2} \frac{\partial r_2}{\partial x} = 0, \tag{3.65}$$

$$\frac{\partial U}{\partial y} = \frac{\partial U}{\partial r_1} \frac{\partial r_1}{\partial y} + \frac{\partial U}{\partial r_2} \frac{\partial r_2}{\partial y} = 0 \tag{3.66}$$

using the form of $U = U(r_1, r_2)$ given in Eq. (3.64). Evaluating the partial derivatives, we can write the equations for the location of the equilibrium points as

$$\mu_1 \left( -\frac{1}{r_1^2} + r_1 \right) \frac{x + \mu_2}{r_1} + \mu_2 \left( -\frac{1}{r_2^2} + r_2 \right) \frac{x - \mu_1}{r_2} = 0, \tag{3.67}$$

$$\mu_1 \left( -\frac{1}{r_1^2} + r_1 \right) \frac{y}{r_1} + \mu_2 \left( -\frac{1}{r_2^2} + r_2 \right) \frac{y}{r_2} = 0. \tag{3.68}$$

Inspection of Eqs. (3.65) and (3.66) shows the existence of the trivial solution

$$\frac{\partial U}{\partial r_1} = \mu_1 \left( -\frac{1}{r_1^2} + r_1 \right) = 0, \qquad \frac{\partial U}{\partial r_2} = \mu_2 \left( -\frac{1}{r_2^2} + r_2 \right) = 0, \tag{3.69}$$

which gives $r_1 = r_2 = 1$ in our system of units. Using Eqs. (3.8) and (3.9) this implies

$$(x + \mu_2)^2 + y^2 = 1, \qquad (x - \mu_1)^2 + y^2 = 1 \tag{3.70}$$

with the two solutions

$$x = \frac{1}{2} - \mu_2, \qquad y = \pm \frac{\sqrt{3}}{2}. \tag{3.71}$$

Since $r_1 = r_2 = 1$, each of the two points defined by these equations forms an equilateral triangle with the masses $\mu_1$ and $\mu_2$. These are the *triangular Lagrangian equilibrium points* referred to in Sect. 3.5 as $L_4$ and $L_5$. By convention the leading triangular point is taken to be $L_4$ and the trailing point $L_5$. The analysis given in Sect. 3.5 rules out any additional off-axis equilibrium points.

It is clear from Eq. (3.68) that $y = 0$ is a simple solution of Eq. (3.66), implying that the remaining equilibrium points lie along the $x$ axis and satisfy Eq. (3.65). There are, in fact, three such solutions corresponding to the *collinear Lagrangian equilibrium points* denoted by $L_1$, $L_2$, and $L_3$. The $L_1$ point lies between the masses $\mu_1$ and $\mu_2$, the $L_2$ point lies outside the mass $\mu_2$, and the $L_3$ point lies on the negative $x$ axis. We now derive an approximate location for each of the collinear points.

At the $L_1$ point we have

$$r_1 + r_2 = 1, \quad r_1 = x + \mu_2, \quad r_2 = -x + \mu_1, \quad \frac{\partial r_1}{\partial x} = -\frac{\partial r_2}{\partial x} = 1. \tag{3.72}$$

Hence, substituting in Eq. (3.67) gives us

$$\mu_1 \left( -\frac{1}{(1 - r_2)^2} + 1 - r_2 \right) - \mu_2 \left( -\frac{1}{r_2^2} + r_2 \right) = 0 \tag{3.73}$$

or

$$\frac{\mu_2}{\mu_1} = 3 r_2^3 \frac{(1 - r_2 + r_2^2/3)}{(1 + r_2 + r_2^2)(1 - r_2)^3}. \tag{3.74}$$

If we define

$$\alpha = \left(\frac{\mu_2}{3\mu_1}\right)^{1/3} \tag{3.75}$$

then for small $r_2$ it is clear that there is a solution close to $r_2 = \alpha$. We will see later on (see Sect. 3.13) that $\alpha$ is a parameter that occurs naturally in Hill's equations, an approximation to the equations of motion in the vicinity of $\mu_2$. From Eq. (3.74) we have

$$\alpha = r_2 + \frac{1}{3}r_2^2 + \frac{1}{3}r_2^3 + \frac{53}{81}r_2^4 + \mathcal{O}(r_2^5). \tag{3.76}$$

We can use Lagrange's inversion method (see Sect. 2.5) to invert this series and express $r_2$ as a function of $\alpha$. Comparing Eq. (3.76) with Eq. (2.89) we can write

$$r_2 = \alpha + (-1/3)\,\phi(r_2), \tag{3.77}$$

where the function $\phi$ is defined by

$$\phi(r_2) = r_2^2 + r_2^3 + \frac{53}{27}r_2^4 + \mathcal{O}(r_2^5), \tag{3.78}$$

and hence

$$[\phi(\alpha)]^2 = \alpha^4 + 2\alpha^5 + \mathcal{O}(\alpha^6), \tag{3.79}$$

$$\frac{\mathrm{d}}{\mathrm{d}\alpha}[\phi(\alpha)]^2 = 4\alpha^3 + 10\alpha^4 + \mathcal{O}(\alpha^5), \tag{3.80}$$

$$[\phi(\alpha)]^3 = \alpha^6 + \mathcal{O}(\alpha^7), \tag{3.81}$$

$$\frac{\mathrm{d}^2}{\mathrm{d}\alpha^2}[\phi(\alpha)]^3 = 30\alpha^4 + \mathcal{O}(\alpha^5). \tag{3.82}$$

Therefore, using these expressions and Eq. (2.90) we have

$$\begin{aligned} r_2 &= \alpha + \sum_{j=1}^{\infty} \frac{(-1/3)^j}{j!} \frac{\mathrm{d}^{j-1}}{\mathrm{d}\alpha^{j-1}} [\phi(\alpha)]^j \\ &= \alpha - \frac{1}{3}\alpha^2 - \frac{1}{9}\alpha^3 - \frac{23}{81}\alpha^4 + \mathcal{O}(\alpha^5). \end{aligned} \tag{3.83}$$

At the $L_2$ point we have

$$r_1 - r_2 = 1, \quad r_1 = x + \mu_2, \quad r_2 = x - \mu_1, \quad \frac{\partial r_1}{\partial x} = \frac{\partial r_2}{\partial x} = 1. \tag{3.84}$$

Hence substituting for $r_1$ in Eq. (3.67) we have

$$\mu_1\left(-\frac{1}{(1+r_2)^2} + 1 + r_2\right) + \mu_2\left(-\frac{1}{r_2^2} + r_2\right) = 0 \tag{3.85}$$

or

$$\frac{\mu_2}{\mu_1} = 3r_2^3 \frac{(1 + r_2 + r_2^2/3)}{(1+r_2)^2(1 - r_2^3)}. \tag{3.86}$$

Using the definition of $\alpha$ in Eq. (3.75) gives us

$$\alpha = r_2 - \frac{1}{3}r_2^2 + \frac{1}{3}r_2^3 + \frac{1}{81}r_2^4 + \mathcal{O}(r_2^5), \tag{3.87}$$

$$r_2 = \alpha + \frac{1}{3}\alpha^2 - \frac{1}{9}\alpha^3 - \frac{31}{81}\alpha^4 + \mathcal{O}(\alpha^5). \tag{3.88}$$

At the $L_3$ point we have

$$r_2 - r_1 = 1, \quad r_1 = -x - \mu_2, \quad r_2 = -x + \mu_1, \quad \frac{\partial r_1}{\partial x} = \frac{\partial r_2}{\partial x} = -1. \tag{3.89}$$

Hence substituting for $r_2$ in Eq. (3.67) gives us

$$\mu_1\left(-\frac{1}{r_1^2} + r_1\right) + \mu_2\left(-\frac{1}{(1+r_1)^2} + 1 + r_1\right) = 0 \tag{3.90}$$

or

$$\frac{\mu_2}{\mu_1} = \frac{(1-r_1^3)(1+r_1)^2}{r_1^3(r_1^2+3r_1+3)}. \tag{3.91}$$

If we let $r_1 = 1 + \beta$ (which implies $r_2 = 2 + \beta$) we then have

$$\frac{\mu_2}{\mu_1} = -\frac{12}{7}\beta + \frac{144}{49}\beta^2 - \frac{1567}{343}\beta^3 + \mathcal{O}(\beta^4), \tag{3.92}$$

$$\beta = -\frac{7}{12}\left(\frac{\mu_2}{\mu_1}\right) + \frac{7}{12}\left(\frac{\mu_2}{\mu_1}\right)^2 - \frac{13223}{20736}\left(\frac{\mu_2}{\mu_1}\right)^3 + \mathcal{O}\left(\frac{\mu_2}{\mu_1}\right)^4. \tag{3.93}$$

The locations of all the Lagrangian points and zero-velocity curves for three critical values of the Jacobi constant for a mass ratio $\mu_2 = 0.2$ are shown in Fig. 3.7. In Fig. 3.8 the surface defined by the zero-velocity curves is shown for the same mass ratio.

Referring to Figs. 3.7 and 3.8 we see that the $L_1$ point has the largest value of the Jacobi constant ($C_\mathrm{J} = 3.805$ for $\mu_2 = 0.2$) and lies at a critical point of the innermost curve. There is another branch of the same curve (approximately circular in shape) that lies beyond the $L_2$ point. It is clear from a comparison with Fig. 3.2 that the $L_1$ point separates those trajectories confined to orbits either around the primary or the secondary from those that can orbit both masses (cf. Fig. 3.2). The $L_2$ point ($C_\mathrm{J} = 3.552$ for $\mu_2 = 0.2$) is another saddle point on the zero-velocity curve. A particle with $C_\mathrm{J} < C_{L_2}$ could orbit in the interior or exterior regions of the plane. Two branches of the zero-velocity curves also meet at the $L_3$ point ($C_\mathrm{J} = 3.197$ for $\mu_2 = 0.2$). The triangular equilibrium points $L_4$ and $L_5$ have the lowest value of the Jacobi constant ($C_\mathrm{J} = 2.84$ for $\mu_2 = 0.2$); if

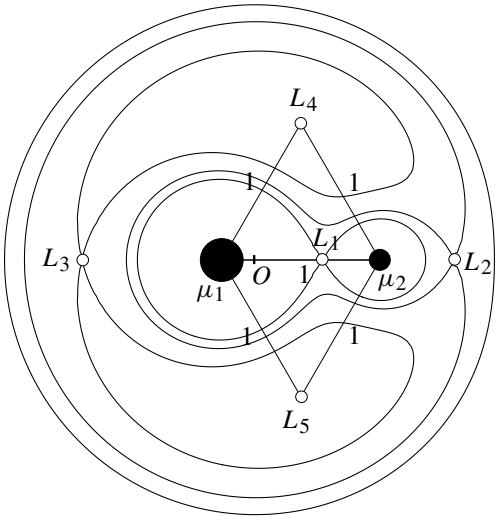


Fig. 3.7. The location of the Lagrangian equilibrium points (denoted by the small, open circles) and associated zero-velocity curves for $\mu_2 = 0.2$. The plot shows the zero-velocity curves for the three critical values of the Jacobi constant (3.805, 3.552, 3.197) that pass through the points $L_1$, $L_2$, and $L_3$ for this value of $\mu_2$. The point $O$ denotes the centre of mass of the system.

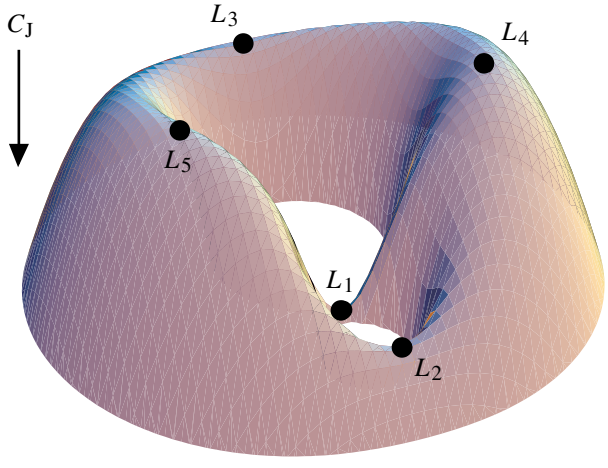


Fig. 3.8. The three-dimensional surface defined by $C_J = 2U$ and the location of the Lagrangian equilibrium points for $\mu_2 = 0.2$, the same as that used in Fig. 3.7. The points $L_1$, $L_2$, and $L_3$ all lie at saddle points on the surface. The surface is drawn such that the vertical height represents the negative value of the Jacobi constant $C_J$.

a particle has a Jacobi constant $C_J < C_{L_{4,5}}$ then there are no regions of the plane from which it is excluded. This does not imply that the particle will travel to all accessible regions, only that the Jacobi constant cannot provide bounds to the motion.

There is no universally accepted ordering system for the Lagrangian equilibrium points, although it is customary for $L_4$ and $L_5$ to denote the leading and trailing triangular points respectively. We choose to label the points according to the value of the Jacobi constant at the equilibrium point, from the largest (at $L_1$) to the smallest (at $L_4$ and $L_5$). We can calculate these values of the Jacobi constant using a series expansion of Eq. (3.39) (taking $n = 1$) with the appropriate values for $x$ and $y$, or $r_1$ and $r_2$, as derived above. Including terms up to $\mathcal{O}(\mu_2)$ in the expansion, this gives

$$C_{L_1} \approx 3 + 3^{4/3}\mu_2^{2/3} - 10\mu_2/3, \tag{3.94}$$

$$C_{L_2} \approx 3 + 3^{4/3}\mu_2^{2/3} - 14\mu_2/3, \tag{3.95}$$

$$C_{L_3} \approx 3 + \mu_2, \tag{3.96}$$

$$C_{L_4} \approx 3 - \mu_2, \tag{3.97}$$

$$C_{L_5} \approx 3 - \mu_2. \tag{3.98}$$

Note that Eqs. (3.8), (3.9), and (3.39) are identical if $y$ is replaced with $-y$ and hence the zero-velocity curves must be symmetric about the $x$ axis (this is already clear from Figs. 3.2 and 3.7), and thus the values of the Jacobi constant at the $L_4$ and $L_5$ points are the same.

The largest value of $\mu_2 = m_2/(m_1+m_2)$ in the solar system occurs in the Pluto–Charon system where $\mu_2 \approx 10^{-1}$. The Earth–Moon system has $\mu_2 \approx 10^{-2}$ but all other planet–satellite and Sun–planet pairs have values at least an order of magnitude smaller. Therefore, since we are interested in applications to the solar system, it is important to consider the shape of the zero-velocity curves and the positions of the Lagrangian equilibrium points for small values of $\mu_2$.

From Eqs. (3.94) and (3.95) it is clear that as $\mu_2 \to 0$, $C_{L_1} \to C_{L_2}$. Also, from Eqs. (3.83) and (3.88), we see that as $\mu_2 \to 0$ the terms of $\mathcal{O}(\alpha^2)$ and higher can be neglected and $L_1$ and $L_2$ become equidistant from the mass $\mu_2$. The $L_3$ point lies at a distance of $1 + \beta$ from the central mass, where $\beta$ ($< 0$) is given by Eq. (3.93). Therefore, as $\mu_2 \to 0$ the $L_3$ point approaches the unit circle. The triangular points already lie on the unit circle centred on the mass $\mu_1$ and are at a distance $r = (1 - \mu_2 + \mu_2^2)^{1/2}$ from the centre of mass. Since the quantity $\mu_2$ is also the distance between the mass $\mu_1$ and the centre of mass of the system, as $\mu_2 \to 0$ the unit circle centred on $\mu_1$ approaches the unit circle centred on the centre of mass.

Figure 3.9 shows a selection of zero velocity curves and the locations of the Lagrangian equilibrium points for the case where $\mu_2 = 0.01$, a value comparable

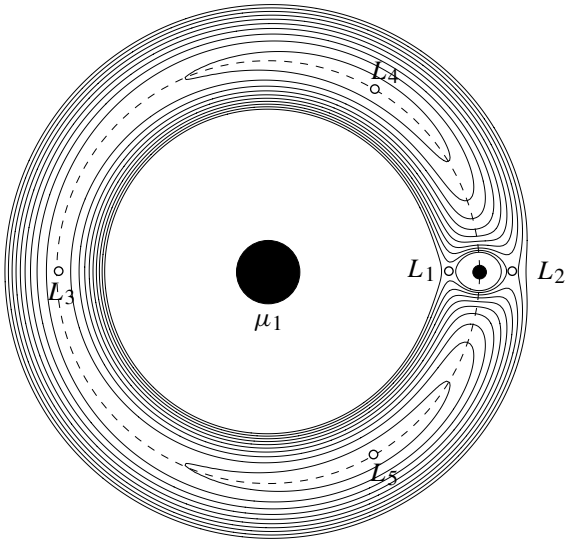


Fig. 3.9. The location of the Lagrangian equilibrium points (open circles) and associated zero-velocity curves for a mass $\mu_2 = 0.01$. The dashed line denotes the circle of unit radius centred on the mass $\mu_1$.

to that in the Earth–Moon system. Note that the $L_1$ and $L_2$ points are almost equidistant from the mass $\mu_2$ and that the $L_3$ point lies close to the unit circle. Although the dashed line in Fig. 3.9 denotes the unit circle centred on the mass $\mu_1$, a shift of 1% of its radius to the right would produce a unit circle centred on the centre of mass.

To illustrate the degree of symmetry about the unit circle when $\mu_2 \to 0$ we have calculated the radial distances of the individual equilibrium points from the centre of mass of the system for values of $\mu_2$ between $10^{-1}$ and $10^{-10}$ (see Fig. 3.10). The results show the approach of first $L_3$, $L_4$, and $L_5$, and then $L_1$ and $L_2$, to the unit radius as $\mu_2 \to 0$. This property of the zero-velocity curves and the equilibrium points allows us to make useful approximations when discussing the motion of the test particle in the case of a system with a small mass ratio.

## 3.7 Stability of Equilibrium Points

It is not enough to know that a number of equilibrium points exist for a dynamical system; we also need to determine the stability of such points. When a system is subjected to a force derived from a potential, the sum of the kinetic energy and potential energy remains constant. In such a system "stable" motion occurs at equilibrium positions that are potential minima. Objects placed at these positions will remain in the vicinity despite small displacements. We can demonstrate this by considering a test object given a small displacement from an equilibrium position at a potential minimum. Since the potential energy must increase away from

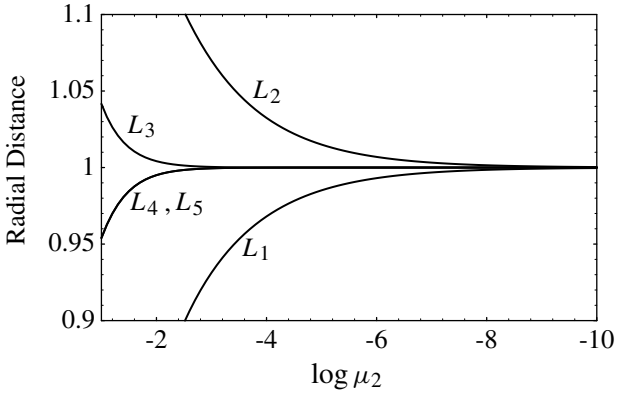


Fig. 3.10. The radial distance of the five Lagrangian equilibrium points from the centre of mass as a function of $\log \mu_2$.

the minimum, the kinetic energy must decrease until it reaches zero. However, the sum of the two forms of energy has to be a constant and so at this point the motion has to reverse, leading to an increase in kinetic energy and a decrease in potential energy. In the presence of a dissipative force that opposes the motion the particle moves towards the equilibrium position. Note, however, that in the case of two-body motion such a drag force actually increases the speed of the orbiting particle because loss of energy implies a decrease in orbital radius and hence an increase in orbital speed.

Consider the zero-velocity curves in the vicinity of a triangular equilibrium point. We have already shown that $C_J = 2U - v^2$ is a minimum at $L_4$ and $L_5$. If we adopted the convention of making the quantity $U$ negative by transforming to a function $U^* = -U$ (see Eqs. (3.23) and (3.24)), then we would make $C_J$ a maximum at the triangular points. However, all that really matters is the direction of motion of the particle and this is not determined by convention. Figure 3.11 shows two zero-velocity curves for the case $\mu_2 = 0.1$. At various points around each curve we have used Eqs. (3.16) and (3.17) to calculate values of the acceleration, $(\ddot{x}, \ddot{y})$, of the particle in the rotating reference frame; although $\dot{x} = \dot{y} = 0$ (since the curves are zero-velocity curves) the vector $(\ddot{x}, \ddot{y})$ is nonzero and is related to the initial direction of the particle's velocity. Notice that this vector is always perpendicular to the zero-velocity curve and that its magnitude, on a given zero-velocity curve, is largest in the vicinity of the triangular point.

Since all the directions of the initial velocity vectors in Fig. 3.11 are pointing away from the $L_4$ point and towards those regions associated with higher values of $C_J$, it would be natural to assume that the point is an unstable equilibrium point. However, appearances can be deceptive and in order to carry out a proper study of the stability we need to examine the behaviour of a particle that is given

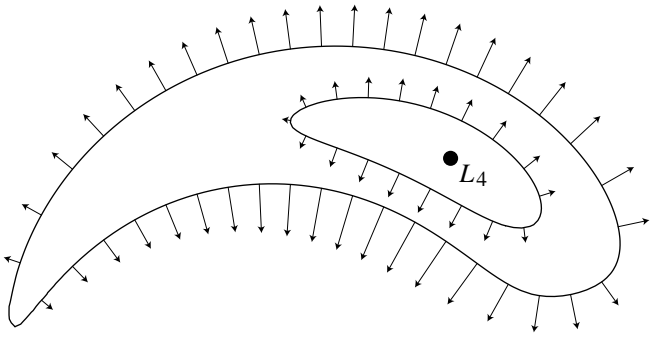


Fig. 3.11. The relative magnitudes and directions of initial motion around two zero-velocity curves ($C_J = 2.95$ and $C_J = 3.09$) in the vicinity of the $L_4$ point for the case $\mu_2 = 0.1$.

a small displacement from an equilibrium position. We can do this by linearising the equations of motion and carrying out a *linear stability analysis.*

Let the location of an equilibrium point in the circular restricted problem be denoted by $(x_0, y_0)$ and consider a small displacement $(X, Y)$ from the point such that $x = x_0 + X$ and $y = y_0 + Y$. Then, by substituting in Eqs. (3.19) and (3.20), and expanding in a Taylor series, we have

$$\begin{aligned}\ddot{X} - 2n\dot{Y} &\approx \left(\frac{\partial U}{\partial x}\right)_0 + X\left(\frac{\partial}{\partial x}\left(\frac{\partial U}{\partial x}\right)\right)_0 + Y\left(\frac{\partial}{\partial y}\left(\frac{\partial U}{\partial x}\right)\right)_0 \\ &= X\left(\frac{\partial^2 U}{\partial x^2}\right)_0 + Y\left(\frac{\partial^2 U}{\partial x \partial y}\right)_0 \end{aligned} \tag{3.99}$$

and

$$\begin{aligned}\ddot{Y} + 2n\dot{X} &\approx \left(\frac{\partial U}{\partial y}\right)_0 + X\left(\frac{\partial}{\partial x}\left(\frac{\partial U}{\partial y}\right)\right)_0 + Y\left(\frac{\partial}{\partial y}\left(\frac{\partial U}{\partial y}\right)\right)_0 \\ &= X\left(\frac{\partial^2 U}{\partial x \partial y}\right)_0 + Y\left(\frac{\partial^2 U}{\partial y^2}\right)_0, \end{aligned} \tag{3.100}$$

where the subscript 0 denotes evaluation of the partial derivatives at the equilibrium point and we have used the fact that $(\partial U/\partial x)_0 = (\partial U/\partial y)_0 = 0$ (recall that the equilibrium points are derived by solving the equations $\partial U/\partial x = \partial U/\partial y = 0$). We are only interested in the motion in the immediate vicinity of the equilibrium point, and so it is legitimate to neglect the higher order terms since these will always be small quantities, providing we only consider a small initial displacement from the point $(x_0, y_0)$; obviously the assumption no longer holds if the displacement is too large. From our initial set of nonlinear differential equations, we have carried out a standard procedure to *linearise* the equations of motion.

The end result is a set of linear differential equations of the form

$$\ddot{X} - 2\dot{Y} = XU_{xx} + YU_{xy}, \qquad \ddot{Y} + 2\dot{X} = XU_{xy} + YU_{yy}, \tag{3.101}$$

where we have taken $n = 1$ and the quantities

$$U_{xx} = \left(\frac{\partial^2 U}{\partial x^2}\right)_0, \quad U_{xy} = \left(\frac{\partial^2 U}{\partial x \partial y}\right)_0, \quad U_{yy} = \left(\frac{\partial^2 U}{\partial y^2}\right)_0 \tag{3.102}$$

are all constants. These equations can be solved using a number of standard techniques, and since similar equations will arise in different circumstances elsewhere in this book, it is worthwhile examining their solution in some detail.

We can write the equations in matrix form as

$$\begin{pmatrix} \dot{X} \\ \dot{Y} \\ \ddot{X} \\ \ddot{Y} \end{pmatrix} = \begin{pmatrix} 0 & 0 & 1 & 0 \\ 0 & 0 & 0 & 1 \\ U_{xx} & U_{xy} & 0 & 2 \\ U_{xy} & U_{yy} & -2 & 0 \end{pmatrix} \begin{pmatrix} X \\ Y \\ \dot{X} \\ \dot{Y} \end{pmatrix}, \tag{3.103}$$

thereby changing the problem to the solution of four, simultaneous, first-order differential equations instead of two, simultaneous, second-order differential equations. The equations now have the form

$$\dot{\mathbf{X}} = \mathbf{A}\mathbf{X}, \tag{3.104}$$

where

$$\mathbf{X} = \begin{pmatrix} X \\ Y \\ \dot{X} \\ \dot{Y} \end{pmatrix} \quad \text{and} \quad \mathbf{A} = \begin{pmatrix} 0 & 0 & 1 & 0 \\ 0 & 0 & 0 & 1 \\ U_{xx} & U_{xy} & 0 & 2 \\ U_{xy} & U_{yy} & -2 & 0 \end{pmatrix}. \tag{3.105}$$

Before proceeding let us consider a general matrix equation of the form given in Eq. (3.104) where $\mathbf{A}$ is an $n \times n$ matrix of constants and $\mathbf{X}$ is an $n$-dimensional vector with elements $X_i$ $(i = 1, 2, \ldots n)$.

If any vector $\mathbf{x}$ satisfies the equation

$$\mathbf{A}\mathbf{x} = \lambda\mathbf{x}, \tag{3.106}$$

where $\lambda$ is a scalar constant, then $\mathbf{x}$ is said to be an *eigenvector* of the matrix $\mathbf{A}$ and $\lambda$ is its corresponding *eigenvalue*. If $\mathbf{A}$ is thought of as a transformation matrix, then the result of applying $\mathbf{A}$ to the particular vector $\mathbf{x}$ satisfying Eq. (3.106) is to produce a vector in the same direction as $\mathbf{x}$ but of a different magnitude.

The first step in the solution of Eq. (3.104) is to find the eigenvalues of $\mathbf{A}$. We can rewrite Eq. (3.106) as

$$(\mathbf{A} - \lambda\mathbf{I})\mathbf{x} = 0, \tag{3.107}$$

where $\mathbf{I}$ is the $n \times n$ unit matrix. This set of $n$ simultaneous, linear equations in $n$ unknowns (the $n$ elements of $\mathbf{x}$) will have nontrivial solutions provided the

determinant of the matrix $\mathbf{A} - \lambda\mathbf{I}$ is zero. Hence, we must have

$$\det(\mathbf{A} - \lambda\mathbf{I}) = 0. \tag{3.108}$$

This produces the *characteristic equation*, which is a polynomial equation of degree $n$ in $\lambda$ with $n$ possible complex roots. The $n$ corresponding eigenvectors can be found by substituting each $\lambda$ into Eq. (3.106) and solving for the components of each $\mathbf{x}$.

Now let us return to the differential equations given in Eq. (3.104). The equations are *coupled*, in the sense that the equation for the time derivative of a general element $X_i$ depends, in general, on various elements of the vector. For example, in our own problem, the equation for the time variation of $\dot{X}$ is a function of $X$, $Y$, and $\dot{Y}$. The equations would be much easier to solve if the coupling could be removed by a suitable transformation to a new set of $n$ variables, $Y_i$, $(i = 1, 2, \ldots n)$ say, where $\dot{Y}_i$ is a function of $Y_i$ alone. This can be achieved by a standard technique known as a *similarity transformation*. Let the transformation from $\mathbf{X}$ to $\mathbf{Y}$ be represented by

$$\mathbf{Y} = \mathbf{B}\mathbf{X}, \tag{3.109}$$

where the constant matrix $\mathbf{B}$ has yet to be determined. We have

$$\mathbf{X} = \mathbf{B}^{-1}\mathbf{Y} \qquad \text{and} \qquad \dot{\mathbf{X}} = \mathbf{B}^{-1}\dot{\mathbf{Y}}, \tag{3.110}$$

where $\mathbf{B}^{-1}$ is the inverse of the matrix $\mathbf{B}$. Hence Eq. (3.104) can be written

$$\mathbf{B}^{-1}\dot{\mathbf{Y}} = \mathbf{A}\mathbf{B}^{-1}\mathbf{Y} \tag{3.111}$$

or, premultiplying each side by $\mathbf{B}$,

$$\dot{\mathbf{Y}} = \mathbf{B}\mathbf{B}^{-1}\dot{\mathbf{Y}} = \mathbf{B}\mathbf{A}\mathbf{B}^{-1}\mathbf{Y}. \tag{3.112}$$

We want the new differential equations given in Eq. (3.112) to be uncoupled. This can be achieved if the matrix $\mathbf{B}$ is chosen such that

$$\mathbf{B}\mathbf{A}\mathbf{B}^{-1} = \mathbf{\Lambda}, \tag{3.113}$$

where $\mathbf{\Lambda}$ denotes a diagonal matrix (i.e., a matrix with all elements not on the leading diagonal equal to zero). It can easily be shown that if the columns of the matrix $\mathbf{B}$ are constructed from the $n$ (column) eigenvectors of the matrix $\mathbf{A}$, then the resulting matrix $\mathbf{\Lambda}$ is a diagonal matrix composed of the eigenvalues of $\mathbf{A}$ with

$$\mathbf{\Lambda} = \begin{pmatrix} \lambda_1 & 0 & \cdots & 0 \\ 0 & \lambda_2 & \cdots & 0 \\ \vdots & \vdots & \ddots & \vdots \\ 0 & 0 & \cdots & \lambda_n \end{pmatrix}. \tag{3.114}$$

The transformed system of equations is now

$$\dot{\mathbf{Y}} = \mathbf{\Lambda}\mathbf{Y} \tag{3.115}$$

or, alternatively, in component form,

$$\dot{Y}_i = \lambda_i Y_i \quad (i = 1, 2, \ldots, n). \tag{3.116}$$

The solutions of Eq. (3.116) are easily found; they are

$$Y_i = c_i e^{\lambda_i t} \quad (i = 1, 2, \ldots, n), \tag{3.117}$$

where the $c_i$ are $n$ constants of integration. However, although the solution of the equations in the $Y_i$ is relatively simple, we must now transform back to obtain our solutions in terms of our original variables, $X_i$. From Eq. (3.110) we have

$$\mathbf{X} = \mathbf{B}^{-1}\mathbf{Y} = \mathbf{B}^{-1} \begin{pmatrix} c_1 e^{\lambda_1 t} \\ c_2 e^{\lambda_2 t} \\ \vdots \\ c_n e^{\lambda_n t} \end{pmatrix}. \tag{3.118}$$

The $n$ constants of integration, $c_i$, can now be determined from the starting values by solving the $n$ simultaneous, linear equations given in Eq. (3.118).

We can now apply the method given above to our problem. In our case $n = 4$ and the characteristic equation is given by

$$\det(\mathbf{A} - \lambda\mathbf{I}) = \begin{vmatrix} -\lambda & 0 & 1 & 0 \\ 0 & -\lambda & 0 & 1 \\ U_{xx} & U_{xy} & -\lambda & 2 \\ U_{xy} & U_{yy} & -2 & -\lambda \end{vmatrix} = 0, \tag{3.119}$$

which reduces to the polynomial equation

$$\lambda^4 + (4 - U_{xx} - U_{yy})\lambda^2 + U_{xx}U_{yy} - U_{xy}^2 = 0. \tag{3.120}$$

This is a quartic in the variable $\lambda$ but it is also a *biquadratic*, or a quadratic equation in $\lambda^2$. This makes it relatively easy to find the four roots. They are

$$\lambda_{1,2} = \pm\left[\frac{1}{2}(U_{xx} + U_{yy} - 4) - \frac{1}{2}\left[(4 - U_{xx} - U_{yy})^2 - 4(U_{xx}U_{yy} - U_{xy}^2)\right]^{1/2}\right]^{1/2} \tag{3.121}$$

and

$$\lambda_{3,4} = \pm\left[\frac{1}{2}(U_{xx} + U_{yy} - 4) + \frac{1}{2}\left[(4 - U_{xx} - U_{yy})^2 - 4(U_{xx}U_{yy} - U_{xy}^2)\right]^{1/2}\right]^{1/2}. \tag{3.122}$$

Although our general solution given in Eq. (3.118) appears to involve knowing the four eigenvectors of $\mathbf{A}$, in practice this is not required. It is clear from

Eq. (3.118) that we can write the solution for $X$ and $\dot{X}$ as

$$X = \sum_{j=1}^{4} \bar{\alpha}_j e^{\lambda_j t}, \qquad \dot{X} = \sum_{j=1}^{4} \bar{\alpha}_j \lambda_j e^{\lambda_j t}, \tag{3.123}$$

where the $\bar{\alpha}_j$ are constants. Similarly we can derive expressions for $Y$ and $\dot{Y}$ in terms of constants $\bar{\beta}_j$. We have

$$Y = \sum_{j=1}^{4} \bar{\beta}_j e^{\lambda_j t}, \qquad \dot{Y} = \sum_{j=1}^{4} \bar{\beta}_j \lambda_j e^{\lambda_j t}, \tag{3.124}$$

where the constants $\bar{\beta}_j$ are functions of the $\bar{\alpha}_j$ since there can only be four constants in the solution. The relationship between the $\bar{\alpha}_j$ and the $\bar{\beta}_j$ can be derived from either of the equations in Eq. (3.101). Substituting the expressions for $X$, $Y$, and $\dot{Y}$ into Eq. (3.101) we have

$$\sum_{j=1}^{4} \left( \bar{\alpha}_j \lambda_j^2 - 2\bar{\beta}_j \lambda_j - U_{xx} \bar{\alpha}_j - U_{xy} \bar{\beta}_j \right) e^{\lambda_j t} = 0. \tag{3.125}$$

The trivial solution of this equation gives the relationship between the $\bar{\alpha}_j$ and the $\bar{\beta}_j$:

$$\bar{\beta}_j = \frac{\lambda_j^2 - U_{xx}}{2\lambda_j + U_{xy}} \bar{\alpha}_j. \tag{3.126}$$

If, at time $t = 0$, we have the boundary conditions $X = X_0$, $Y = Y_0$, $\dot{X} = \dot{X}_0$, and $\dot{Y} = \dot{Y}_0$, then the four $\bar{\alpha}_j$ (and hence the related $\bar{\beta}_j$) are determined from the solution of the four simultaneous linear equations

$$\sum_{j=1}^{4} \bar{\alpha}_j = X_0, \qquad \sum_{j=1}^{4} \lambda_j \bar{\alpha}_j = \dot{X}_0, \qquad \sum_{j=1}^{4} \bar{\beta}_j = Y_0, \qquad \sum_{j=1}^{4} \lambda_j \bar{\beta}_j = \dot{Y}_0. \tag{3.127}$$

Although the complete solution is described by Eqs. (3.123) and (3.124) with the constants $\bar{\alpha}_j$ and $\bar{\beta}_j$ given by the solutions to Eqs. (3.127), the stability of the equilibrium points can be determined from an inspection of the eigenvalues alone. To investigate the nature of the eigenvalues we define the quantities

$$\bar{A} = \frac{\mu_1}{(r_1^3)_0} + \frac{\mu_2}{(r_2^3)_0}, \tag{3.128}$$

$$\bar{B} = 3 \left[ \frac{\mu_1}{(r_1^5)_0} + \frac{\mu_2}{(r_2^5)_0} \right] y_0^2, \tag{3.129}$$

$$\bar{C} = 3 \left[ \mu_1 \frac{(x_0 + \mu_2)}{(r_1^5)_0} + \mu_2 \frac{(x_0 - \mu_1)}{(r_2^5)_0} \right] y_0, \tag{3.130}$$

$$\bar{D} = 3 \left[ \mu_1 \frac{(x_0 + \mu_2)^2}{(r_1^5)_0} + \mu_2 \frac{(x_0 - \mu_1)^2}{(r_2^5)_0} \right]. \tag{3.131}$$

In terms of these constants we can write

$$U_{xx} = 1 - \bar{A} + \bar{D}, \tag{3.132}$$

$$U_{yy} = 1 - \bar{A} + \bar{B}, \tag{3.133}$$

$$U_{xy} = \bar{C}. \tag{3.134}$$

Note that all of these quantities are real numbers and that $X$, $Y$, $\dot{X}$, and $\dot{Y}$ must also be real, even though the eigenvalues $\lambda_j$ and the constants $\bar{\alpha}_j$ and $\bar{\beta}_j$ can be complex.

The general form of the eigenvalues given by Eqs. (3.121) and (3.122) is

$$\lambda_{1,2} = \pm(j_1 + \mathrm{i}k_1), \qquad \lambda_{3,4} = \pm(j_2 + \mathrm{i}k_2), \tag{3.135}$$

where $j_1$, $k_1$, $j_2$, and $k_2$ are real quantities and $\mathrm{i} = \sqrt{-1}$. Given that the form of the general solution for the components of the position and velocity vectors relative to the equilibrium point (see Eqs. (3.123) and (3.124)) involves a linear combination of terms of the form $\mathrm{e}^{\lambda_j t}$, this implies that each of the two $\mathrm{e}^{+(j+\mathrm{i}k)t}$ terms will be matched by an $\mathrm{e}^{-(j+\mathrm{i}k)t}$ term. If $j = 0$ then an oscillatory solution will result because terms with $\mathrm{e}^{+\mathrm{i}kt}$ and $\mathrm{e}^{-\mathrm{i}kt}$ will reduce to sines and cosines (since $\mathrm{e}^{\pm\mathrm{i}\theta} = \cos\theta \pm \mathrm{i}\sin\theta$). However, if $j$ is positive then there will always be exponential growth in at least one mode and so the perturbed solution is unstable. Therefore the equilibrium point is stable if all the eigenvalues are purely imaginary. We will see how this works in practice by considering the general and specific cases.

### 3.7.1 The Collinear Points

Consider the collinear solutions corresponding to the Lagrangian points $L_1$, $L_2$, and $L_3$. For these points we have $y_0 = 0$, $(r_1^2)_0 = (x_0 + \mu_2)^2$, and $(r_2^2)_0 = (x_0 - \mu_1)^2$, and hence

$$U_{xx} = 1 + 2\bar{A}, \qquad U_{yy} = 1 - \bar{A}, \qquad U_{xy} = 0. \tag{3.136}$$

The characteristic equation becomes

$$\lambda^4 + (2 - \bar{A})\lambda^2 + (1 + \bar{A} - 2\bar{A}^2) = 0. \tag{3.137}$$

As a specific example consider the stability of the $L_1$ point for the case when $\mu_2 = 0.01$ using the theory developed in Sect. 3.6. From Sect. 3.6 we have $x_0 = 0.848$ and $y_0 = 0$; we will assume an initial displacement of $X_0 = Y_0 = 10^{-5}$ and take $\dot{X}_0 = \dot{Y}_0 = 0$. The resulting eigenvalues are $\pm 2.90$ and $\pm 2.32\mathrm{i}$, indicating that the point is linearly unstable. Solving for the $\bar{\alpha}_j$ and $\bar{\beta}_j$ we derive the solution

$$\begin{aligned} X(t) &= 6.99 \times 10^{-6}\mathrm{e}^{-2.90t} + 4.96 \times 10^{-6}\mathrm{e}^{+2.90t} \\ &\quad + 1.96 \times 10^{-6}\cos 2.32t + 2.54 \times 10^{-6}\sin 2.32t, \\ Y(t) &= 3.25 \times 10^{-6}\mathrm{e}^{-2.90t} - 2.31 \times 10^{-6}\mathrm{e}^{+2.90t} \\ &\quad + 9.06 \times 10^{-6}\cos 2.32t + 6.96 \times 10^{-6}\sin 2.32t. \end{aligned} \tag{3.138}$$

The second term in each of these equations will eventually dominate and lead to exponential growth in the $X$ and $Y$. The e-folding timescale for growth in this case is $1/2.90$ orbital periods of the mass $\mu_2$.

The nonzero values of the real and imaginary parts of the solutions to the quartic for the case of the $L_1$ point are shown in Fig. 3.12 for values of $\mu_2$ between 0.1 and 0.001. Notice, as in the specific case shown above, that the roots are always of the form $\pm j$ and $\pm \mathrm{i}k$, where $j$ and $k$ are real quantities. A similar plot can be obtained for $L_2$ and $L_3$ but with different numerical values.

From the properties of polynomials we know that the product of the roots must equal the constant term in the polynomial. Hence the characteristic equation must satisfy

$$(\lambda_1\lambda_2)(\lambda_3\lambda_4) = 1 + \bar{A} - 2\bar{A}^2, \tag{3.139}$$

where, from Eqs. (3.121) and (3.122), $\lambda_1 = -\lambda_2$ and $\lambda_3 = -\lambda_4$. In order for all the roots to be purely imaginary (the condition for stability) we must have $\lambda_1^2 = \lambda_2^2 < 0$ and $\lambda_3^2 = \lambda_4^2 < 0$; this implies that $1+\bar{A}-2\bar{A}^2 = (1-\bar{A})(1+2\bar{A}) > 0$. Therefore the collinear points are stable provided $-1/2 < \bar{A} < 1$. However, substituting the values of $r_1$ and $r_2$ for the collinear points into Eq. (3.128) shows that $\bar{A} > 1$ (given that $\mu_2 < 1/2$) and so the collinear points are unstable for all values of $\mu_2$. In fact the solution will always have the form given in Eq. (3.138) but with decreasing values of the eigenvalues as the mass decreases (see Fig. 3.12). Physically we can understand the existence of the unstable collinear points by considering the changes in gravitational acceleration and centrifugal force at different locations along the $x$ axis. Moving away from both masses gravity drops off and the centrifugal acceleration increases. Thus

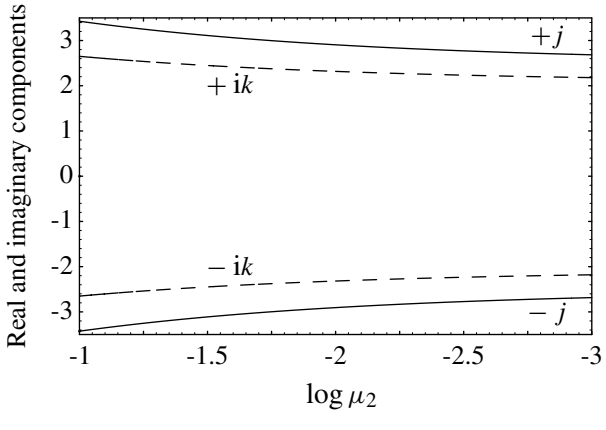


Fig. 3.12. Numerical values of the real (solid lines) and imaginary (dashed lines) components of the roots of the characteristic equation for the $L_1$ Lagrangian point as a function of the value of $\mu_2$.

there are exactly two equilibrium points with $m_1$ and $m_2$ between them. Similar reasoning shows that there is just one equilibrium point between the two masses. The force on a particle anywhere along the $x$ axis is directed away from these equilibrium points and hence they are all unstable.

However, with special starting conditions it is possible to find stable, periodic orbits in the vicinity of the equilibrium points (see, for example, Szebehely 1967). In fact, the *SOHO* spacecraft (Domingo et al. 1995) was placed in such an orbit near the $L_1$ point in the Earth–Sun system in order to observe the Sun continuously.

### 3.7.2 The Triangular Points

Now consider the motion in the vicinity of $L_4$ and $L_5$. In this case, $r_1 = r_2 = 1$, $x = 1/2 - \mu_2$, $y = \pm\sqrt{3}/2$, and we have

$$U_{xx} = 3/4, \qquad U_{yy} = 9/4, \qquad U_{xy} = \pm 3\sqrt{3}(1 - 2\mu_2)/4. \tag{3.140}$$

The characteristic equation becomes

$$\lambda^4 + \lambda^2 + \frac{27}{4}\mu_2(1 - \mu_2) = 0. \tag{3.141}$$

As above we now consider a specific example. At the $L_4$ point with $\mu_2 = 0.01$ we have $x_0 = 0.49$ and $y_0 = \sqrt{3}/2$ with the same initial conditions as before. The resulting eigenvalues are $\pm 0.963$i and $\pm 0.268$i, indicating that the point is linearly stable. The solution for the perturbed motion is

$$\begin{aligned} X(t) &= 3.45 \times 10^{-5} \cos 0.268t - 2.45 \times 10^{-5} \cos 0.963t \\ &\quad + 3.07 \times 10^{-4} \sin 0.268t - 8.55 \times 10^{-5} \sin 0.963t, \\ Y(t) &= 5.20 \times 10^{-5} \cos 0.268t - 4.20 \times 10^{-5} \cos 0.963t \\ &\quad - 1.76 \times 10^{-4} \sin 0.268t + 4.90 \times 10^{-5} \sin 0.963t. \end{aligned} \tag{3.142}$$

Therefore the solution is of the oscillatory type with fundamental periods of $1/0.268$ and $1/0.963$ orbital periods of the orbiting body.

Figure 3.13 shows how the nature of the eigenvalues varies with the mass. It is clear that the eigenvalues have real parts for values of $\mu_2$ larger than a critical value ($\log \mu_2 \approx -1.4$). In this case the eigenvalues are of the form $\pm j \pm \mathrm{i}k$ and so there will always be a positive real part. However, provided the mass is small enough the eigenvalues are always of the form $\pm \mathrm{i}k_1$ and $\pm \mathrm{i}k_2$, and the perturbed motion is stable.

We can understand the behaviour shown in Fig. 3.13 by considering the analytical solutions to the characteristic equation. Substituting the expressions for

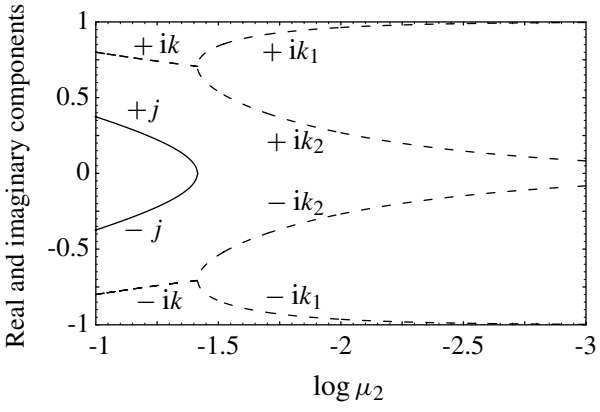


Fig. 3.13. Numerical values of the real (solid lines) and imaginary (dashed lines) components of the roots of the characteristic equation for the $L_4$ and $L_5$ Lagrangian points as a function of the value of $\mu_2$. Note the change in the nature of the eigenvalues at $\log \mu_2 \approx -1.4$.

$U_{xx}$, $U_{yy}$, and $U_{xy}$ into Eqs. (3.121) and (3.122) gives

$$\lambda_{1,2} = \pm \frac{\sqrt{-1 - \sqrt{1 - 27(1-\mu_2)\mu_2}}}{\sqrt{2}} \tag{3.143}$$

and

$$\lambda_{3,4} = \pm \frac{\sqrt{-1 + \sqrt{1 - 27(1-\mu_2)\mu_2}}}{\sqrt{2}}. \tag{3.144}$$

Therefore all the eigenvalues will be purely imaginary if and only if the condition

$$1 - 27(1-\mu_2)\mu_2 \geq 0$$

is satisfied. This implies that the condition for linear stability reduces to

$$\mu_2 \leq \frac{27 - \sqrt{621}}{54} \approx 0.0385. \tag{3.145}$$

When the eigenvalues are purely imaginary they will occur in pairs of the form $\lambda_{1,2} = \pm \mathrm{i} k_1$ and $\lambda_{3,4} = \pm \mathrm{i} k_2$, where $k_1$ and $k_2$ are real numbers. If we write $\bar{\alpha}_j = \bar{a}_j + \mathrm{i}\bar{b}_j$, where $\bar{a}_j$ and $\bar{b}_j$ are real, then, from (3.123), the solution for $X(t)$ is of the form

$$\begin{aligned} X(t) = {} & (\bar{a}_1 + \mathrm{i}\bar{b}_1)\mathrm{e}^{+\mathrm{i}k_1 t} + (\bar{a}_2 + \mathrm{i}\bar{b}_2)\mathrm{e}^{-\mathrm{i}k_1 t} \\ & + (\bar{a}_3 + \mathrm{i}\bar{b}_3)\mathrm{e}^{+\mathrm{i}k_2 t} + (\bar{a}_4 + \mathrm{i}\bar{b}_4)\mathrm{e}^{-\mathrm{i}k_2 t}, \end{aligned} \tag{3.146}$$

with a similar equation for $Y(t)$. We can use Eq. (3.127) and the fact that $X$, $Y$, $\dot{X}$, and $\dot{Y}$ must all be real to show that $\bar{a}_1 = \bar{a}_2 = a_1$, $\bar{a}_3 = \bar{a}_4 = a_2$, $\bar{b}_1 = -\bar{b}_2 = b_1$,

and $\bar{b}_3 = -\bar{b}_4 = b_2$ and the coefficients of the exponential terms consist of pairs of complex conjugates. Hence our solution for $X(t)$ can be written

$$X(t) = (a_1 + \mathrm{i}b_1)\mathrm{e}^{+\mathrm{i}k_1 t} + (a_1 - \mathrm{i}b_1)\mathrm{e}^{-\mathrm{i}k_1 t} + (a_2 + \mathrm{i}b_2)\mathrm{e}^{+\mathrm{i}k_2 t} + (a_2 - \mathrm{i}b_2)\mathrm{e}^{-\mathrm{i}k_2 t}. \tag{3.147}$$

Since $\mathrm{e}^{\mathrm{i}\theta} = \cos\theta + \mathrm{i}\sin\theta$ and the coefficients are complex conjugates this can be rewritten as

$$X(t) = 2a_1 \cos k_1 t + 2a_2 \cos k_2 t - 2b_1 \sin k_1 t - 2b_2 \sin k_2 t. \tag{3.148}$$

Therefore, if the eigenvalues are purely imaginary the resulting motion of the particle displaced from the equilibrium point is oscillatory in form; hence the particle will remain in the vicinity of the equilibrium point and the motion is stable. This confirms the numerical result given above.

If the condition in Eq. (3.145) is not satisfied then the eigenvalues have real parts and have the form $\pm(j \pm \mathrm{i}k)$ (see the left part of Fig. 3.13). In this case we can write

$$X(t) = (a_1 + \mathrm{i}b_1)\mathrm{e}^{(j+\mathrm{i}k)t} + (a_1 - \mathrm{i}b_1)\mathrm{e}^{(j-\mathrm{i}k)t} + (a_2 + \mathrm{i}b_2)\mathrm{e}^{(-j+\mathrm{i}k)t} + (a_2 - \mathrm{i}b_2)\mathrm{e}^{(-j-\mathrm{i}k)t}, \tag{3.149}$$

which reduces to

$$X(t) = 2\left(a_1\mathrm{e}^{jt} + a_2\mathrm{e}^{-jt}\right)\cos kt - 2\left(b_1\mathrm{e}^{jt} + b_2\mathrm{e}^{-jt}\right)\sin kt. \tag{3.150}$$

Therefore there will always be exponential growth in the variable $X$ arising from at least two of the terms. The same is true for the expressions for $Y$, $\dot{X}$, and $\dot{Y}$. This results in a trajectory that spirals away from the equilibrium point and hence the point is said to be linearly unstable.

Now let us return to our analysis of the stable case ($\mu_2 < 0.0385$). From Eqs. (3.143) and (3.144) we see that for small values of $\mu_2$ the eigenvalues can be written

$$\lambda_{1,2} \approx \pm\sqrt{-1 + \frac{27}{4}\mu_2}, \qquad \lambda_{3,4} \approx \pm\sqrt{-\frac{27}{4}\mu_2}. \tag{3.151}$$

These are both purely imaginary numbers for small mass ratios and we have seen numerically and analytically that the moduli of these values of $\lambda$ are the two frequencies of the motion of the particle in its oscillations about the triangular equilibrium point. The existence of these two frequencies in the solution to the perturbed motion near the $L_4$ and $L_5$ points gives rise to a further problem, which reduces the generality of the condition shown in Eq. (3.145). The possible existence of *resonances* (i.e., simple numerical relationships) between these frequencies means that for a finite number of specific mass ratios the points are unstable, even though the relationship in Eq. (3.145) is satisfied (Deprit & Deprit-Bartholomé 1967).

## 3.8 Motion near $L_4$ and $L_5$

We have chosen a system of units such that the mean motion of the mass $\mu_2$ is unity and its orbital period is $2\pi$. The corresponding periods of the particle motion are $2\pi/|\lambda_{1,2}|$ and $2\pi/|\lambda_{3,4}|$. Therefore the resulting motion of the particle is composed of two different motions:

- a short-period motion with a period $2\pi/|\lambda_{1,2}| \approx 2\pi$ (i.e., a period that is close to the orbital period of the mass $\mu_2$) and
- a superimposed longer period motion of period $2\pi/|\lambda_{3,4}|$, known as a *libration*, about the equilibrium point.

The amplitudes of these motions are determined by the constants $\bar{\alpha}_j$ and $\bar{\beta}_j$, which are in turn determined by the starting conditions. In this context the motion can be thought of as a long-period motion of an epicentre around the equilibrium point with the particle simultaneously executing a short-period motion around the epicentre (see Fig. 3.14). The resulting motion of the particle for the numerical solution given by Eq. (3.142) is shown in Fig. 3.15.

The peculiar, looping nature of the particle's path shown in Fig. 3.15 results from the two different types of motion that contribute to the perturbed orbit about the equilibrium point. The nature of this motion can be further simplified by rotating the coordinate system by 30° ($\pi/6$ radians) clockwise about the equilibrium point such that the transformed $X$ axis is nearly tangential to the unit circle. The new coordinates, $(X', Y')$, are given by

$$\begin{pmatrix} X'(t) \\ Y'(t) \end{pmatrix} = \begin{pmatrix} \cos 30^\circ & -\sin 30^\circ \\ \sin 30^\circ & \cos 30^\circ \end{pmatrix} \begin{pmatrix} X(t) \\ Y(t) \end{pmatrix}, \tag{3.152}$$

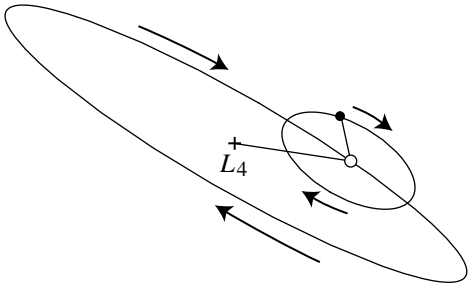


Fig. 3.14. The epicyclic motion (small ellipse) and the motion of the epicentre (large ellipse) for the solution given in Eq. (3.142). The epicentre is denoted by the small empty circle. The cross denotes the location of the $L_4$ equilibrium point. The particle's path around the equilibrium is a combination of the epicyclic motion and the motion of the epicentre.

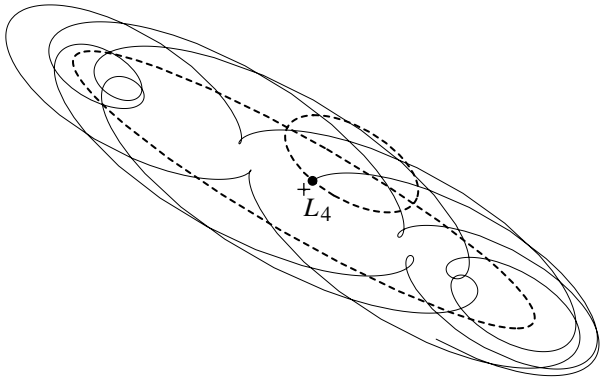


Fig. 3.15. The trajectory in the rotating frame of a particle librating about the $L_4$ Lagrangian equilibrium point. The trajectory is derived from the analytical solution to the stability problem given in Eq. (3.142) and the motion is shown for $25\pi$ time units (12.5 orbital periods of the mass $\mu_2$). The dashed lines denote the epicyclic motion and the path of the epicentre shown in Fig. 3.14.

where $X(t)$ and $Y(t)$ are given by Eq. (3.142). Hence

$$\begin{aligned} X'(t) &\approx 3.54 \times 10^{-4} \sin 0.268t - 9.85 \times 10^{-5} \sin 0.963t, \\ Y'(t) &\approx 6.23 \times 10^{-5} \cos 0.268t - 4.86 \times 10^{-5} \cos 0.963t. \end{aligned} \tag{3.153}$$

Although the values of the constants (apart from the frequencies) in these equations depend on the specific boundary conditions, the rotation serves to highlight several additional properties of the orbital solution. By separating the two types of motion we see that each is of the form given in Eq. (2.40) and so each describes a centred ellipse. In the case of the motion of the epicentre the path is an elongated ellipse. In Sect. 3.10 we will show that the dimensions of this ellipse are determined by the dimensions of the *associated zero-velocity curve* and that the ratio of the semi-minor and semi-major axes is given by $b/a = (3\mu_2)^{1/2}$.

For the epicyclic motion around the epicentre the particle traces a path that is a centred ellipse with semi-major and semi-minor axes in the approximate ratio 2:1. Given that we are considering the path in a rotating frame, this motion is identical to the epicycle or guiding centre approximation to the two-body problem described in Sect. 2.6. Therefore we can think of the epicyclic motion as the regular keplerian motion from pericentre to apocentre that produces a centred ellipse with semi-axes of length $2e$ and $e$. In our particular case this suggests that we have $e \approx 5 \times 10^{-5}$. The actual situation is not quite so simple and we have to consider the osculating eccentricity of the particle as a combination of a "forced" eccentricity from the mass $\mu_2$ (reflected in part by the changing shape of the elongated ellipse of the epicentre's path) and a "free" eccentricity giving the 2:1 epicyclic motion. We will return to this concept in Chapter 7 when we consider secular perturbations. We note in passing that by a judicious

choice of starting conditions it is possible to find orbital solutions where the epicyclic motion is entirely suppressed and the particle's path is just the path of the epicentre.

## 3.9 Tadpole and Horseshoe Orbits

It is important to remember that the types of motion described by the solution of the equations for perturbed motion around $L_4$ and $L_5$ are only valid in the vicinity of these equilibrium points and, by implication, only for small amplitudes of libration. This means that we cannot deduce anything about the solution for large displacements from the equilibrium points. However, it is always possible to resort to numerical integration of the full equations of motion of the particle in the rotating frame; these were derived in Sect. 3.2 (see Eqs. (3.16) and (3.17)).

Figure 3.16 shows two separate trajectories obtained by integrating the full equations of motion for starting conditions in the vicinity of the $L_4$ point for $\mu_2 = 0.001$, a value similar to the Sun–Jupiter mass ratio. The trajectory shown in Fig. 3.16a has been started slightly closer to $L_4$ than the one shown in Fig. 3.16b. Note that in each case the path is more elongated ahead of the $L_4$ point. Furthermore, in Fig. 3.16a the orbit extends over 86°; the orbit that was started further from $L_4$ shown in Fig. 3.16b extends over 115°. Recalling that the two masses and $L_4$ form an equilateral triangle, the side of which is the unit of length, it is clear from Fig. 3.16 that both orbits move close to the unit circle centred on the mass $\mu_1$ (cf. Fig. 3.9). The orbits shown in Fig. 3.16 are referred to as *tadpole orbits* because of the elongated shapes of the orbits (and the zero-velocity curves). The similarity is even more enhanced when orbits with zero free eccentricity are considered. Note that tadpole orbits also describe particle paths around the $L_5$ point.

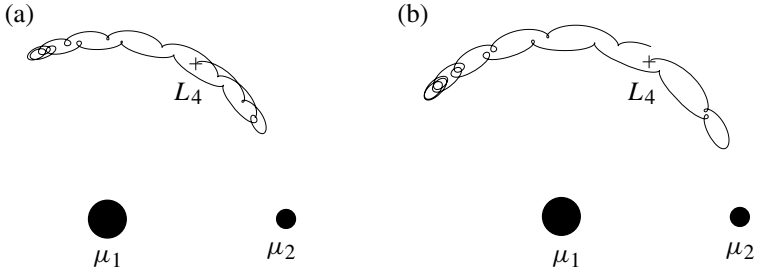


Fig. 3.16. Two examples of tadpole orbits librating about the $L_4$ equilibrium point (denoted by a cross and located at $x_0 = 1/2 - \mu_2$, $y_0 = \sqrt{3}/2$) for $\mu_2 = 0.001$. The masses $\mu_1$ and $\mu_2$ are denoted by the filled circles. (a) The starting conditions are $x = x_0 + 0.0065$, $y = y_0 + 0.0065$ with $\dot{x} = \dot{y} = 0$ and the orbit is followed for 15 orbital periods of $\mu_2$. (b) The starting conditions are $x = x_0 + 0.008$, $y = y_0 + 0.008$ with $\dot{x} = \dot{y} = 0$ and the orbit is followed for 15.5 orbital periods of $\mu_2$.

The question now arises as to what kind of orbit would we expect if we increase the initial radial separation from $L_4$ or $L_5$ even more? The answer is that provided the initial distance is not too large, the resulting orbit will encompass both $L_4$ and $L_5$. These are referred to as *horseshoe orbits* and two examples are shown in Fig. 3.17 using starting conditions taken from the paper by Taylor (1981). Note that the orbit shown in Fig. 3.17b has starting conditions that almost suppress the epicyclic motion, giving a smooth appearance to the path.

Comparison of the paths of the epicentres deduced from Figs. 3.16 and 3.17 with the form of the zero-velocity curves shown in Fig. 3.9 reveals striking similarities. However, it is important to note that the zero-velocity curves do not define the orbital paths, although, as we shall see in Sect. 3.10, there is a close connection between the two when $\mu_2$ is small. Note that those orbits shown in Figs. 3.16 and 3.17 have zero initial velocities. Hence there is a zero-velocity curve associated with each of the orbits, although these have not been drawn. Such curves only guarantee that the orbits do not get too close to the $L_4$ and $L_5$ points and give no indication of the long-term stability of the orbits. However, remember that if the Jacobi constant of an orbit is less than that for $L_4$ and $L_5$, then a zero-velocity curve cannot be drawn and there are no excluded regions.

We can illustrate the properties of horseshoe and tadpole orbits for small mass ratios with a number of examples obtained from direct numerical integrations of the equations of motion. Figure 3.18 shows three trajectories (one horseshoe and two tadpole) for the case where $\mu_2 = 10^{-3}$. Here $\theta$ is the angle around the orbit, with $\theta = 0$ corresponding to the line from the primary mass to the secondary mass. All the orbits are started with eccentricity $e \approx 0$. Note that there is considerable variation of the semi-major axis around the orbit with the

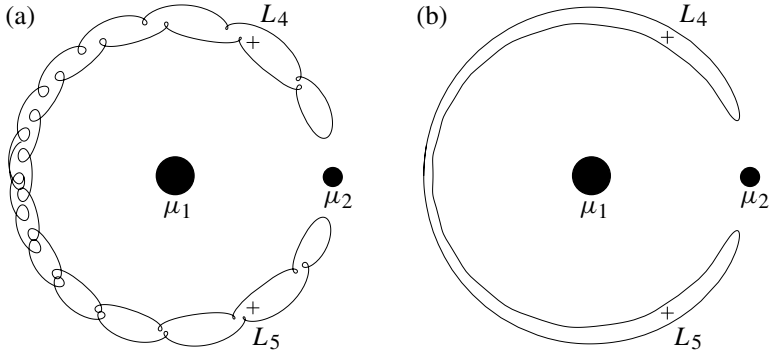


Fig. 3.17. Two examples of near-periodic horseshoe orbits librating about the $L_4$ equilibrium point for $\mu_2 = 0.000953875$, taken from data given by Taylor (1981). (a) The starting conditions are $x = -0.97668$, $y = \dot{x} = 0$, $\dot{y} = -0.06118$. (b) The starting conditions are $x = -1.02745$, $y = \dot{x} = 0$, $\dot{y} = 0.04032$.

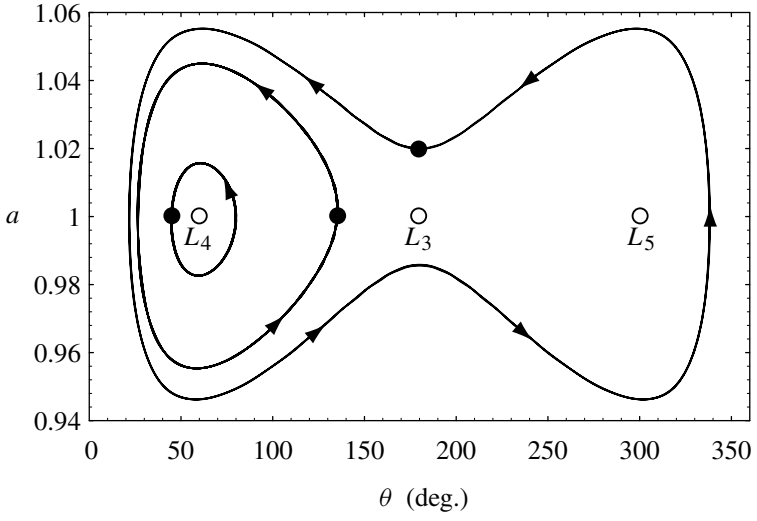


Fig. 3.18. The variation of semi-major axis $a$ with the angle $\theta$ around the orbit for three trajectories with $\mu_2 = 10^{-3}$. The starting positions are indicated by filled circles and the enclosed equilibrium points with open circles. All orbits were followed for 100 orbital periods of the secondary mass and arrows indicate the direction of the motion.

maximum deviation from the unit circle occurring at the $L_4$ and $L_5$ equilibrium points. At these points the horseshoe and tadpoles have their maximum width. Note too that there is considerable asymmetry in the path. This is demonstrated by the fact that the $L_3$ point does not lie midway between the outer and inner branches of the horseshoe at $\theta = 180^\circ$. Although we are plotting the variation of $a$ and not $r$ around the path, there would be little difference because we have chosen $e \approx 0$. Therefore the loops apparent in Figs. 3.16 and 3.17 do not appear in this example.

The changes in $a$ and $e$ as a function of time for the horseshoe orbit (with $\mu_2 = 10^{-3}$) are shown in Fig. 3.19. The relatively sudden changes in $a$ denote the effect of encounters with the secondary mass when the orbit switches from $a > 1$ to $a < 1$, or vice versa (see Fig. 3.19a). If we write $a = 1 + \Delta a$ and measure $\Delta a$ every time $\theta = 180^\circ$ then an interesting phenomenon emerges. We chose an initial value of $\Delta a = 0.020$. After one encounter with the secondary $\Delta a = -0.0143$, but after two encounters measurements show that $\Delta a = 0.0198$, with the pattern repeating itself at subsequent encounters. This demonstrates that the asymmetry in $|\Delta a|$ is almost cancelled out after one complete cycle of the horseshoe. As we shall see in Sect. 3.15, this property can be useful in maintaining horseshoe orbits against the orbital decay produced by dissipation (Dermott et al. 1980, Dermott & Murray 1981a). It is clear from Fig. 3.19b that

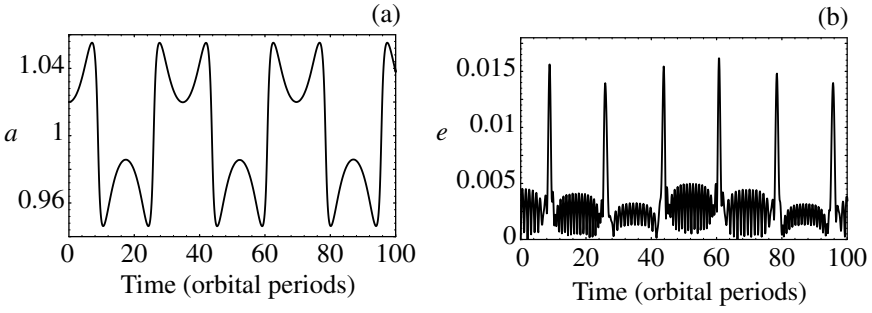


Fig. 3.19. The variation of (a) semi-major axis $a$, and (b) eccentricity $e$ as a function of time for the horseshoe orbit shown in Fig. 3.18 for $\mu_2 = 10^{-3}$.

the encounters with the secondary also correspond to times of sudden changes in $e$, with an order of magnitude increase on approach and decrease on retreat. The small oscillations in eccentricity between encounters (which, in accordance with Tisserand's relation also have a maximum amplitude at the $L_4$ and $L_5$ points) imply that phase effects could be important. This helps to explain why there are variations in the magnitude of the eccentricity "impulse" at encounters, rather than the symmetry (after two encounters) shown in the variation in $a$.

The effect of a decrease in the mass ratio is shown in Figs. 3.20 and 3.21, where we show two of the equivalent plots for the case $\mu_2 = 10^{-6}$. Because of the decrease in $\mu_2$ we have chosen the initial semi-major axis to be $a = 1.002$, (i.e., a value of $\Delta a$ that is an order of magnitude smaller). The plot of the variation of $a$ with $\theta$ shows, as before, that the paths have maximum width in $a$ at $\theta = 60^\circ$ and $\theta = 300^\circ$, the locations of the $L_4$ and $L_5$ points. However, there are two subtle differences. Firstly, the degree of symmetry is more pronounced with $L_3$ now lying approximately midway between the values of $a$ at $\theta = 180^\circ$. Secondly, although we have started both tadpoles with the same values of $\theta$ as before ($135^\circ$ and $45^\circ$) they have a smaller relative extent in $a$ than their counterparts for $\mu_2 = 10^{-3}$. This implies that the radial extent of the tadpole zone with respect to the horseshoe zone has decreased with decreasing $\mu_2$. For the tadpole orbit we have added its zero-velocity curve for comparison. Note that its radial width is always half that of the tadpole orbit, in keeping with our analytical result.

The extent of symmetry in the small-$\mu_2$ case is clearly shown in Fig. 3.21. The integration shows that that while initially $\Delta a = 0.00200$, after one encounter $\Delta a = -0.00199$, and after two encounters $\Delta a = 0.00200$. If the long-term stability of a horseshoe orbit can be deduced from its proximity to a symmetric periodic orbit then this suggests that horseshoe orbits in the small-$\mu_2$ case are highly stable. Examination of the changes in $e$ shows that order of magnitude

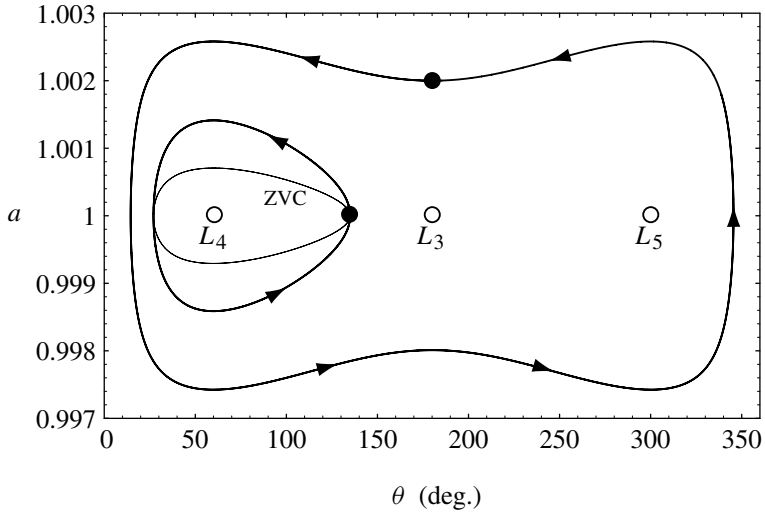


Fig. 3.20. The variation of semi-major axis $a$ with the angle $\theta$ around the orbit for horseshoe and tadpole trajectories with $\mu_2 = 10^{-6}$. The starting positions are indicated by filled circles and the enclosed equilibrium points with open circles. The zero-velocity curve for the tadpole trajectory is the thin curve labelled ZVC. All orbits were followed for 1,000 orbital periods of the secondary mass and arrows indicate the direction of the motion.

changes still occur at encounters but the symmetry is much more pronounced than in the large $\mu_2$ case.

If a starting condition is chosen that corresponds to a near-circular orbit either interior or exterior to the unit circle, then it is clear that the nature of the resulting orbit depends on the radial separation of the orbit from the unit circle. We have shown analytically and numerically how particles started close

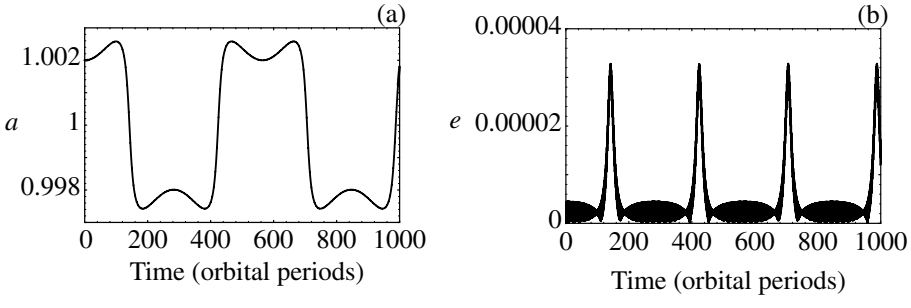


Fig. 3.21. The variation of (a) semi-major axis $a$, and (b) eccentricity $e$ as a function of time for the horseshoe orbit shown in Fig. 3.20 for $\mu_2 = 10^{-6}$.

to $L_4$ and $L_5$ execute a small-amplitude libration about the equilibrium point. By increasing the initial separation the resulting orbit becomes more elongated in the direction of the $L_3$ point (tadpole orbits). Eventually particles started sufficiently far from the unit circle will librate about $L_4$, $L_3$, and $L_5$ (horseshoe orbits). However, particles moving sufficiently far from the unit circle will not give rise to orbits with a change in the direction of motion of the epicentre and the orbits are said to *circulate* interior or exterior to the unit circle. Depending on the value of the Jacobi constant it may be possible for the particle to encounter the mass $\mu_2$.

## 3.10 Orbits and Zero-Velocity Curves

The zero-velocity curve that defines the limits of the forbidden region in Fig. 3.15 has an elongated shape and is tilted at an angle of $\sim 30^\circ$ to the horizontal. We can study the behaviour of such curves in the vicinity of the triangular equilibrium points by means of a translation of the origin, a rotation of $30^\circ$, and an expansion about the new origin. At the $L_4$ point, for example, we have $x = 1/2 - \mu_2$ and $y = \sqrt{3}/2$. The translation of the origin is achieved with the substitutions $x \to (1/2 - \mu_2) + x$ and $y \to \sqrt{3}/2 + y$ in Eqs. (3.8) and (3.9). A rotation of the coordinate system by $30^\circ$ about the new origin is achieved by a substitution $x \to \sqrt{3}x'/2 + y'/2$ and $y \to -x'/2 + \sqrt{3}y'/2$, where $x'$ and $y'$ are the new values of $x$ and $y$. This gives

$$r_1^2 = 1 + 2y' + x'^2 + y'^2, \tag{3.154}$$

$$r_2^2 = 1 - \sqrt{3}x' + y' + x'^2 + y'^2. \tag{3.155}$$

From Eq. (3.22) the transformed equation defining the zero-velocity curves, $C_\mathrm{J} = 2U$, is given by

$$C_\mathrm{J} = 1 - \mu_2 - \sqrt{3}\mu_2 x' + (2 - \mu_2)y' + x'^2 + y'^2 + 2\left(\frac{(1-\mu_2)}{r_1} + \frac{\mu_2}{r_2}\right), \tag{3.156}$$

where terms of $\mathcal{O}(\mu_2^2)$ have been neglected. Expanding Eq. (3.156) about the new origin we obtain

$$C_\mathrm{J} \approx 3 - \mu_2 + \frac{9}{4}\mu_2 x'^2 + 3y'^2. \tag{3.157}$$

In this expansion we have neglected terms of order three and higher as well as terms involving $\mu_2 y'$ since (i) $\mu_2$ is assumed to be a small quantity and (ii) the shapes of the zero-velocity curves shown in Fig. 3.9 suggest that the radial extent of the curves is small for small $\mu_2$; note that the term in $\mu_2 x$ vanishes without making any approximation. In effect our approximation amounts to neglecting the curvature of the resulting curves along the unit radius. If we write

$$C_\mathrm{J} = 3 + \gamma\mu_2, \tag{3.158}$$

where $\gamma$ is a small quantity equal to $-1$ at the $L_4$ and $L_5$ points (see Eqs. (3.97) and (3.98)), then Eq. (3.157) can be written

$$\frac{x'^2}{(4/9)(1+\gamma)} + \frac{y'^2}{(\mu_2/3)(1+\gamma)} = 1. \tag{3.159}$$

If we compare this with Eq. (2.40) we see that the resulting zero-velocity curves are ellipses centred on the $L_4$ point with $a' = (2/3)\sqrt{1+\gamma}$ and $b' = \sqrt{\mu_2/3}\sqrt{1+\gamma}$ as the values of the semi-major and semi-minor axes respectively. Since $b'/a' = (1/2)\sqrt{3\mu_2}$ it is clear that these ellipses become highly elongated as $\mu_2 \to 0$. Note also that the expression for $b'/a'$ is twice the value we gave in Sect. 3.8 for the motion of the guiding centre, suggesting that it is the shape of the zero-velocity curve that determines the particle path. We now investigate the relationship between the zero-velocity curves and the actual orbits in the case where $\mu_2 \ll \mu_2^{1/2} \ll \mu_2^{1/3} \ll 1$. We also assume that the eccentricity of the particle's orbit is near zero and thus, in effect, that the epicyclic motion of the particle about its guiding centre is negligible.

We start by noting from Eqs. (3.94)–(3.98) that the zero-velocity curves that give rise to the tadpole-shaped curves can be characterised by the quantity $\gamma$ defined in Eq. (3.158), where

$$-1 \le \gamma \le +1\,. \tag{3.160}$$

The lower limit of $\gamma$ corresponds to the value of $C_\mathrm{J}$ at the $L_4$ and $L_5$ points whereas the upper limit corresponds to the value at the $L_3$ point. In the case of the horseshoe-shaped curves we can write

$$C_\mathrm{J} = 3 + \zeta\mu_2^{2/3} + \mathcal{O}(\mu_2), \tag{3.161}$$

where

$$0 \le \zeta \le 3^{4/3}\,. \tag{3.162}$$

In this case the lower limit of $\zeta$ corresponds to the value of $C_\mathrm{J}$ (to $\mathcal{O}(\mu_2)$) at the $L_3$ point and the upper limit to the value at the $L_1$ and $L_2$ points. Therefore the value of either $\gamma$ or $\zeta$ serves to parameterise the tadpole or horseshoe nature of the zero-velocity curve.

Using the particular form of the function $U$ given in Eq. (3.64) and taking $n = 1$ we have

$$2U = 2\frac{\mu_1}{r_1} + \mu_1 r_1^2 + 2\frac{\mu_2}{r_2} + \mu_2 r_2^2 - \mu_1\mu_2 \tag{3.163}$$

with, from Eq. (3.28),

$$v^2 = \dot{r}^2 + (r\dot{\theta})^2 = 2U - C_\mathrm{J}. \tag{3.164}$$

Because we are considering $\mu_2 \ll 1$ we make no distinction between $r_1$ and $r$.

If we now restrict our attention to those orbits that are nearly circular and lie close to the unit circle we can write

$$r = 1 + \delta r, \tag{3.165}$$

where $\delta r \ll 1$. In these circumstances $|\dot{r}| \ll |r\dot{\theta}|$ except near the turning points where we have $\dot{\theta} = 0$ but $\dot{r} \neq 0$. Hence, for most of the time the motion is near-keplerian and

$$v \approx r\dot{\theta} = -\frac{3}{2}\delta r. \tag{3.166}$$

Using the same type of approximations we can simplify the expression for $2U$ given in Eq. (3.163). Including terms up to $\mathcal{O}(\mu_2)$ gives

$$2U = 3 + 3\delta r^2 + \mu_2 H, \tag{3.167}$$

where

$$H = \frac{2}{r_2} + r_2^2 - 4\,. \tag{3.168}$$

Hence, using $v^2 = 2U - C_\mathrm{J}$ and Eq. (3.164), we have

$$\frac{9}{4}\delta r^2 = 3 + 3\delta r^2 + \mu_2 H - C_\mathrm{J}. \tag{3.169}$$

If we consider the equation for the zero-velocity curves then $v^2 = 0$ and the curves are defined by the equation

$$0 = 3 + 3\delta r_\mathrm{zv}^2 + \mu_2 H_\mathrm{zv} - C_\mathrm{J}, \tag{3.170}$$

where the subscript "zv" denotes that the quantities described refer to the zero-velocity curves, not the orbits. Given that $C_\mathrm{J}$ is a constant, Eqs. (3.169) and (3.170) give

$$\delta r^2 = \left(2\delta r_\mathrm{zv}\right)^2 + \frac{4}{3}\mu_2\left(H_\mathrm{zv} - H\right). \tag{3.171}$$

For motion in both tadpole and horseshoe orbits, $H_\mathrm{zv} - H \sim \delta r$ and $\mu_2 \delta r \ll \delta r^2$. Hence, for the motion of the guiding centre

$$\delta r = 2\delta r_\mathrm{zv}, \tag{3.172}$$

and the radial displacement of the guiding centre from the unit circle is always twice that of the associated zero-velocity curve (Dermott & Murray 1981a).

In the case of horseshoe orbits Eqs. (3.161) and (3.162) apply and thus

$$\begin{aligned} 3 + \frac{3}{4}\delta r^2 + \mu_2 H &= 3 + \zeta\mu_2^{2/3} + \mathcal{O}(\mu_2), \\ 3 + 3\delta r_\mathrm{zv}^2 + \mu_2 H_\mathrm{zv} &= 3 + \zeta\mu_2^{2/3} + \mathcal{O}(\mu_2). \end{aligned} \tag{3.173}$$

Hence, since $\mu_2^{2/3} \gg \mu_2$ for small values of $\mu_2$, we have

$$\delta r = 2\delta r_\mathrm{zv} = 2(\zeta/3)^{1/2}\mu_2^{1/3}. \tag{3.174}$$

For tadpole orbits Eqs. (3.158) and (3.160) apply and so

$$3 + \frac{3}{4}\delta r^2 + \mu_2 H = 3 + \gamma\mu_2, \qquad 3 + 3\delta r_{\rm zv}^2 + \mu_2 H_{\rm zv} = 3 + \gamma\mu_2. \tag{3.175}$$

Hence

$$\delta r \approx 2\delta r_{\rm zv} = 2[(\gamma - H)/3]^{1/2}\mu_2^{1/2}, \tag{3.176}$$

and again the radial width of the orbit is twice the width of its associated zero-velocity curve.

We have already seen in Sect. 3.8 that for small oscillations about $L_4$ or $L_5$, the semi-minor axis of the elliptical path of the guiding centre is twice that of the semi-minor axis of the ellipse describing the zero-velocity curve associated with the guiding centre. The argument given above suggests, firstly, that the motion of the particle described numerically in Eq. (3.153) is given by

$$\begin{aligned} X'(t) &= a\sin\lambda_3(t - t_3) - 2e\sin\lambda_1(t - t_1), \\ Y'(t) &= (3\mu_2)^{1/2}a\cos\lambda_3(t - t_3) - e\cos\lambda_1(t - t_1), \end{aligned} \tag{3.177}$$

where $\lambda_1$ and $\lambda_3$ are the two fundamental eigenfrequencies and the four arbitrary constants, $a$, $e$, $t_1$, and $t_3$, are determined by the initial conditions, $X'(0)$, $Y'(0)$, $\dot{X}'(0)$, and $\dot{Y}'(0)$. Secondly, it suggests that for small $e$, the motion of the guiding centre is independent of $e$. Thirdly, and most importantly, it suggests that the relationship between the path of the guiding centre and its associated zero-velocity curve that was first encountered when we considered small oscillations about $L_4$ and $L_5$ is true in general and can be applied to motions of any amplitude including motions in horseshoe orbits. We now use this result to derive further properties of the motion.

Once we consider motion far from $L_4$ or $L_5$, the orbits become more tadpolelike with "tails" extending towards $L_3$. We can calculate the minimum and maximum angular extent of these orbits by making use of the Jacobi constant. Equations (3.173) and (3.175) can be rewritten as

$$\frac{3}{4}\delta r^2 + \mu_2 H(\theta) = \text{ constant}, \tag{3.178}$$

where $\theta$ is the angular separation of the particle from the secondary mass; using the geometry of the isosceles triangle $r_2 = 2\sin\theta/2$ and hence

$$H(\theta) = \left(\sin\frac{\theta}{2}\right)^{-1} - 2\cos\theta - 2, \tag{3.179}$$

where $H$ is the same function as defined in Eq. (3.168). The constant in Eq. (3.178) is $\gamma\mu_2$ for tadpole orbits and $\zeta\mu_2^{2/3}$ for horseshoe orbits.

Consider any two points $(r_i, \theta_i)$ and $(r_j, \theta_j)$ on the particle's path. These polar coordinates must satisfy the relation

$$\delta r_i^2 - \delta r_j^2 = -\frac{4}{3}\mu_2\left[H(\theta_i) - H(\theta_j)\right] \tag{3.180}$$

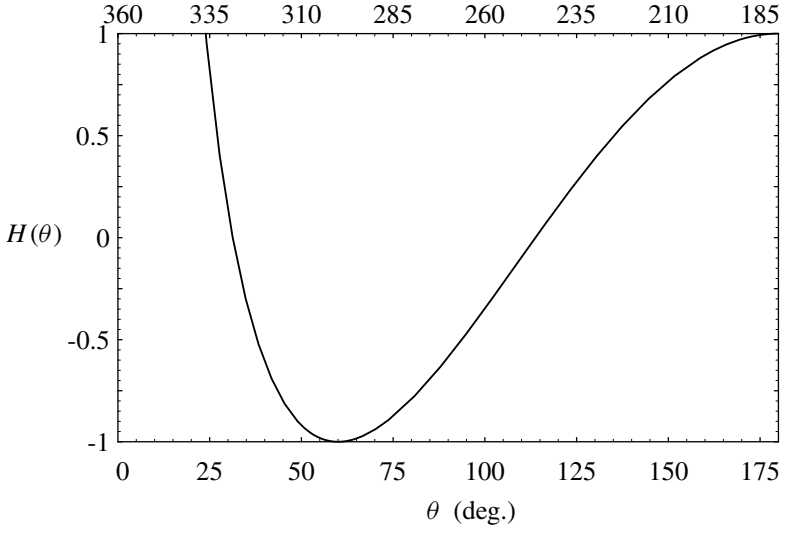


Fig. 3.22. A plot of $H(\theta)$, defined in Eq. (3.179), as a function of $\theta$ for tadpole orbits around $L_4$ (lower scale) and $L_5$ (upper scale).

regardless of whether the particle is in a tadpole or horseshoe orbit. Figure 3.22 shows a plot of $H(\theta)$ as a function of $\theta$. In the case of tadpole orbits we know that at the extremes of the motion $\delta r_i = \delta r_j = 0$ and hence $H(\theta_i) = H(\theta_j)$. The two solutions of this equation, $\theta_{\min}$ and $\theta_{\max}$, give the minimum and maximum angular separations of the particle from the secondary mass, and their difference, $D = \theta_{\max} - \theta_{\min}$, gives the amplitude of the libration. The shape of the $H(\theta)$ curve in Fig. 3.22 helps to explain the observation from our numerical integrations that the tadpole orbits become more elongated at larger amplitudes (see Figs. 3.18 and 3.20).

Consider the case when $\theta_i = 180^\circ$ and $\delta r_i = 0$. This is the orbit of the critical tadpole. With $H(180^\circ) = 1$, Eq. (3.180) gives

$$\delta r_j^2 = \frac{4}{3}\mu_2 \left[1 - H(\theta_j)\right], \tag{3.181}$$

and because $H(\theta) \geq -1$, any tadpole orbit must satisfy the equation

$$\delta r \leq \delta r_{\text{crit}} = \left(\frac{8}{3}\right)^{1/2} \mu_2^{1/2}. \tag{3.182}$$

Therefore, provided $\mu_2$ is known and $e$ is small, a single observation of a $\delta r$ (i.e., the radial separation of the particle from the secondary) is sufficient to determine whether or not the particle moves in a tadpole orbit.

Consider the case when $\theta_i = 180^\circ$ and $\delta r_i = \delta r_{180} \neq 0$. Provided $\zeta \leq 3^{4/3}$ (cf. Eq. (3.162)) the particle is moving on a horseshoe orbit and the turning point of its trajectory occurs when $\delta r_j = 0$ and $\theta_j = \theta_{\min}$. These are related by

$$\delta r_{180}^2 = \frac{4}{3}\mu_2 \left[H(\theta_{\min}) - 1\right], \tag{3.183}$$

and this can be used to determine the closest approach distance between the particle and the secondary and in the case of horseshoe motion an observation of $\theta_{\min}$ could be used to determine the mass $\mu_2$. In the case of tadpole motion $\delta r_{180} = 0$ and $\theta_{\min}$ is given by $H(\theta_{\min}) = 1$ from which we deduce that $\theta_{\min} = 23.5^\circ$ for all $\mu_2$.

## 3.11 Trojan Asteroids and Satellites

The condition Eq. (3.145) is satisfied for every Sun–planet pair in the solar system. The same condition is also satisfied for every planet–satellite pair, with the exception of the Pluto–Charon system where $\mu_2 \sim 0.1$. However, although the behaviour of objects librating about the stable equilibrium points was known to Lagrange, such objects were not discovered until this century. Table 3.1 gives a list of some of the asteroids that are known to move in tadpole orbits about the triangular equilibrium points in the Sun–Jupiter system. These are referred to as the *Trojan asteroids* and the first, (588) Achilles, was discovered in 1906 librating around Jupiter's $L_4$ point.

Up to the end of 1998 more than 450 Trojan asteroids had been discovered librating about Jupiter's $L_4$ and $L_5$ points. The leading ($L_4$) group are commonly referred to as "Greeks" and the trailing ($L_5$) group as "Trojans" with appropriate names taken from the respective sides that are mentioned in Homer's *Iliad* with the added complication of an enemy spy in each camp.

The amplitudes of libration (the quantity $D$ in Table 3.1) can exceed $30^\circ$ but the mean value of the amplitude is $14^\circ$. In such cases the motion of the guiding centre begins to resemble the more elongated zero-velocity curves shown in Fig. 3.9. The physical and dynamical properties of the Trojan asteroids are summarised by Shoemaker et al. (1989).

Figure 3.23 shows the distribution of the Sun–Jupiter Trojan asteroids in December 1997. The projected positions onto the plane of the ecliptic are shown in Fig. 3.23a, together with the orbit and position of Jupiter with respect to the Sun. Although there are two distinct clusterings about the triangular points, the large libration amplitudes are apparent. Figure 3.23b shows the view along the Sun–Jupiter line, illustrating the vertical extent of the Trojan groups.

The presence of Trojan asteroids is not unique to the Sun–Jupiter system: The first Sun–Mars Trojan, (5261) Eureka, was discovered in 1990; Eureka has been shown to be librating about the $L_5$ point of Mars (Mikkola et al. 1994). Asteroid

Table 3.1. Orbital properties of the Trojan asteroids with numbers less than 2,000 that are associated with the Sun–Jupiter system. $D$ is the amplitude of libration; $e_{\rm pr}$ and $I_{\rm pr}$ are the proper eccentricity and inclination respectively as determined by Milani (1993). The final entry indicates whether libration takes place about the $L_4$ or $L_5$ point.

| Asteroid | $D$ (°) | $e_{\rm pr}$ | $\sin I_{\rm pr}$ | $L_4$ | $L_5$ |
|---|---|---|---|---|---|
| (588) Achilles | 6.45 | 0.1032 | 0.1967 | • | |
| (617) Patroclus | 5.02 | 0.1005 | 0.3662 | | • |
| (624) Hektor | 18.99 | 0.0543 | 0.3259 | • | |
| (659) Nestor | 10.03 | 0.1297 | 0.0870 | • | |
| (884) Priamus | 10.82 | 0.0883 | 0.1739 | | • |
| (911) Agamemnon | 16.95 | 0.0207 | 0.3857 | • | |
| (1143) Odysseus | 9.84 | 0.0521 | 0.0689 | • | |
| (1172) Aeneas | 10.15 | 0.0602 | 0.3056 | | • |
| (1173) Anchises | 23.99 | 0.0914 | 0.1404 | | • |
| (1208) Troilus | 10.63 | 0.0354 | 0.5446 | | • |
| (1404) Ajax | 19.98 | 0.0761 | 0.3270 | • | |
| (1437) Diomedes | 28.73 | 0.0179 | 0.3653 | • | |
| (1583) Antilochus | 24.36 | 0.0183 | 0.4858 | • | |
| (1647) Menelaus | 7.93 | 0.0587 | 0.1168 | • | |
| (1749) Telamon | 13.61 | 0.0686 | 0.1185 | • | |
| (1867) Deiphobus | 17.50 | 0.0294 | 0.4738 | | • |
| (1868) Thersites | 22.88 | 0.0979 | 0.2906 | • | |
| (1869) Philoctetes | 21.04 | 0.0576 | 0.0596 | • | |
| (1870) Glaukos | 9.49 | 0.0169 | 0.1114 | | • |
| (1871) Astyanax | 27.76 | 0.0142 | 0.1299 | | • |
| (1872) Helenos | 23.55 | 0.0148 | 0.2538 | | • |
| (1873) Agenor | 12.08 | 0.1168 | 0.3791 | | • |

(3753) Cruithne, originally designated 1986TO, appears to be involved in an unusual horseshoe libration in the Sun–Earth system (Wiegert et al. 1997). Work by Namouni (1999), Christou (1999) and Namouni et al. (1999) shows that the true nature of Cruithne's behaviour, and that of dynamically similar asteroids can be understood in the context of a comprehensive theory of coorbital motion. For example, both Cruithne and (3362) Khufu can become temporary retrograde satellites of Earth whereas 1989VA is involved in a variety of coorbital modes with Venus.

The Trojan asteroids belonging to Jupiter and Mars are examples of librational motion about the $L_4$ and $L_5$ points of Sun–planet systems. However, the dynamics are identical if we also consider motion in the vicinity of the triangular points of a planet–satellite system. These are usually referred to as *coorbital satellites*,

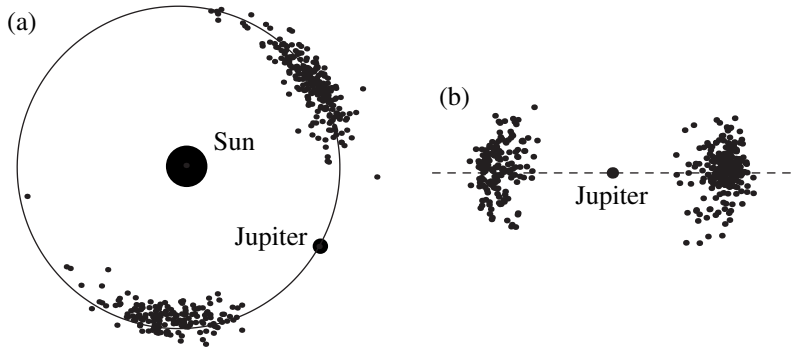


Fig. 3.23. (a) The distribution of asteroids in the vicinity of the orbit of Jupiter on December 18, 1997 at $0^h$ UT (Julian Date 2450800.5). The plot denotes the positions of the asteroids projected onto the plane of the ecliptic. (b) The vertical distribution of the same asteroids viewed along the Jupiter–Sun line. The dashed line denotes the plane of Jupiter's orbit.

although they have also been called *Trojan satellites*. The first coorbital satellites were discovered in 1980 using ground-based CCD observations of the Saturn system. The three objects lie in the orbits of Tethys and Dione (see Table 3.2) and all were directly imaged by the *Voyager* spacecraft during their Saturn flybys in 1980 and 1981.

Although the term *coorbital* was first used to describe the configuration of Janus and Epimetheus (see Sect. 3.12 below), it is now used in connection with any material that shares the same orbit with a larger perturber. Despite the fact that coorbital satellites are common in the saturnian system, it is interesting to note that none exist in the jovian system. A possible explanation for these differences may lie in the relative widths of the tadpole and horseshoe regions.

We have already had some indication of this phenomenon in Sect. 3.9 where we undertook numerical investigations of horseshoe and tadpole orbits for two different mass ratios. Comparing Eqs. (3.174) and (3.176) we see that the width of the horseshoe region is $\sim \mu_2^{1/3}$whereas that of the tadpole region is $\sim \mu_2^{1/2}$.

Table 3.2. A list of known coorbital satellites, the objects involved, and the extent of the libration. The libration entry indicates the extent of motion with respect to the $L_4$ or $L_5$ point.

| Satellite | Primary | Secondary | $\mu_2$ | $L_4$ | $L_5$ | Libration (°) |
|---|---|---|---|---|---|---|
| Telesto | Saturn | Tethys | $1.34 \times 10^{-6}$ | • | | $-2°$ to $+2°$ |
| Calypso | Saturn | Tethys | $1.34 \times 10^{-6}$ | | • | $-4°$ to $+4°$ |
| Helene | Saturn | Dione | $1.85 \times 10^{-6}$ | • | | $-13°$ to $+17°$ |

Therefore the ratio, $R$, of these widths is $\sim \mu_2^{1/6}$ and so $R$ decreases (slowly) as $\mu_2$ decreases. For $\mu_2 \approx 10^{-3}$, $R \approx 0.3$, but for $\mu_2 \approx 10^{-9}$, $R \approx 0.03$. This may explain why horseshoe orbits are more likely for small mass ratios. The lack of any coorbital satellites in the jovian system may be attributable to the larger mass ratios involved, the suggestion being that horseshoe orbits have shorter lifetimes than their tadpole counterparts because they have closer approaches to the perturbing satellite. By considering the evolution of the particle's $|\Delta a|$ after two encounters with the secondary to be a random walk, Dermott & Murray (1981a) estimated that the particles would be lost from the horseshoe configuration on a timescale $\Gamma = T/\mu_2^{5/3}$, where $T$ is the orbital period of the secondary mass.

## 3.12 Janus and Epimetheus

All Trojan asteroids and the above mentioned saturnian satellites are known to be moving in tadpole orbits. However, as shown above, another type of motion is also possible, where libration takes place about $L_4$, $L_5$, and $L_3$ with a guiding centre trajectory similar in shape to some of the zero-velocity curves shown in Fig. 3.9. These are the horseshoe orbits and although they were known to exist in theory and had been studied in numerical experiments, no such orbits had been found in the solar system until relatively recently.

In 1980 two satellites of Saturn, now named Janus and Epimetheus, were imaged by the *Voyager 1* spacecraft. At the time Janus had a semi-major axis $a_J = 151{,}472$ km while Epimetheus, the smaller of the two satellites, had $a_E = 151{,}422$ km (i.e. an orbital separation of 50 km). They have approximate mean diameters of 175 km and 105 km respectively. Since they were $\sim 180^\circ$ apart when they were discovered in February 1980, a naïve analysis would have suggested a collision some time in 1982. However, it was quickly realised that the orbits are performing a variation on the horseshoe solution of the circular restricted problem. Taking $\mu_2 = 5 \times 10^{-9}$ and $\delta r = 3 \times 10^{-4}$, values appropriate for the Janus–Epimetheus system, application of Eq. (3.182) shows that $\delta r > \delta r_{\text{crit}} \approx 17$ km, whereas Eq. (3.174) gives $\zeta = 0.02 < 3^{4/3}$. Therefore we would expect Epimetheus to be moving in a horseshoe orbit.

However, resolved images of the two satellites showed that the mass of Epimetheus could not be considered as negligible compared to that of Janus if their densities are comparable (we now know that their mass ratio is $\sim 0.25$), and therefore mutual perturbations will be important when they approach one another. In fact, as we shall see, approaches between the two satellites lead to a simple modification of the horseshoe configuration. In a reference frame centred on Saturn and rotating with the average mean motion of either satellite, Janus and Epimetheus each librate on their own horseshoe path about longitudes $180^\circ$ apart. If $W_J$ and $W_E$ represent the average widths of the librational arcs of Janus and Epimetheus respectively, then by assuming circular orbits for each satellite

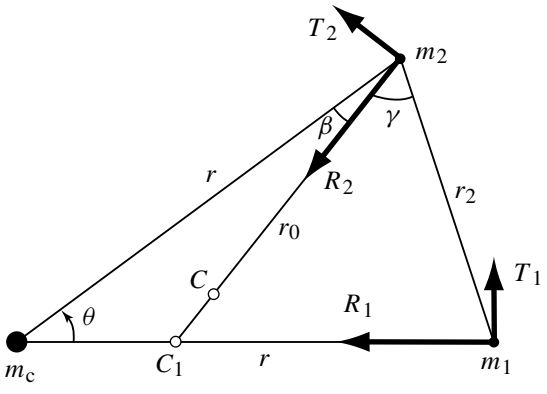


Fig. 3.24. The geometry of the modified horseshoe orbit configuration for two masses $m_1$ and $m_2$ orbiting a central mass $m_c$. $C_1$ is the centre of mass of $m_c$ and $m_1$ while $C$ is the centre of mass of the system. (cf. Fig. 3.6.)

and conservation of the total orbital angular momentum it is easy to show that

$$m_J W_J = m_E W_E. \tag{3.184}$$

We can study the dynamics of this system by taking an approach similar to that in Sect. 3.5. Consider two masses $m_1$ and $m_2$, with $m_2 < m_1$, moving in near-circular orbits with a small radial separation about a central mass $m_c$ (see Fig. 3.24). Let $C_1$ denote the centre of mass of $m_c$ and $m_1$, and $C$ the centre of mass of the system. Note that $C_1$, $C$, and $m_2$ lie on a straight line. The mass $m_2$ experiences an acceleration due to the gravitational attraction of $m_c$ and $m_1$. This can be resolved into a radial component of magnitude $R_2$ directed towards $C$ and a tangential component of magnitude $T_2$ perpendicular to it. We have already seen in Sect. 2.9 (see Eq. (2.149)) that only the tangential component of the force changes the angular momentum of the orbit. Using Eq. (2.145) and assuming $e_2 = 0$ we have, to a good approximation,

$$\dot{a}_2 = 2T_2/n_2, \tag{3.185}$$

where $a_2$ and $n_2$ denote the semi-major axis and the mean motion respectively of $m_2$. Again, we are only concerned with the motion of the guiding centre of the epicycle and we assume that if the free eccentricity is small, then the eccentricity does not have a significant effect on the motion of the guiding centre. The results of numerical experiments support these assumptions.

The tangential acceleration experienced by the mass $m_2$ has contributions from the masses $m_c$ and $m_1$. From Fig. 3.24 this gives

$$T_2 = \left(-\mathcal{G}m_1/r_2^2\right)\sin\gamma + \left(\mathcal{G}m_c/r^2\right)\sin\beta, \tag{3.186}$$

where, from the definitions of $C_1$ and the assumption that $m_2$ is close to the unit circle,

$$\sin\gamma = \frac{m_c}{m_c + m_1}\frac{r}{r_0}\cos\frac{\theta}{2}, \tag{3.187}$$

$$\sin\beta = \frac{m_1}{m_c + m_1}\frac{r}{r_0}\sin\theta, \tag{3.188}$$

and

$$\frac{r}{r_0} = \frac{m_c + m_1}{m_c}\left[1 + 4\frac{m_1}{m_c}\left(\frac{m_c + m_1}{m_c}\right)\sin^2\frac{\theta}{2}\right]^{-1/2} \approx \frac{m_c + m_1}{m_c}. \tag{3.189}$$

Obviously the latter approximation is only good when $\theta$ is small or $m_1 \ll m_c$, but the error does not affect our results. Therefore

$$T_2 = -\left(\mathcal{G}m_1/r^2\right)\bar{H}(\theta), \tag{3.190}$$

where

$$\bar{H}(\theta) = \frac{\cos(\theta/2)}{4\sin^2(\theta/2)} - \sin\theta, \tag{3.191}$$

and we note that $\bar{H}(\theta) = -(1/2)\mathrm{d}H(\theta)/\mathrm{d}\theta$. We can go through a similar procedure to find the tangential acceleration, $T_1$, experienced by the mass $m_1$. This gives

$$T_1 = +\left(\mathcal{G}m_2/r^2\right)\bar{H}(\theta). \tag{3.192}$$

We are now in a position to calculate how the difference in the semi-major axes of the orbiting masses changes with angular separation, $\theta$. Let the difference be

$$s = a_2 - a_1. \tag{3.193}$$

Hence, from Eq. (3.185),

$$\dot{s} = \dot{\theta}\mathrm{d}s/\mathrm{d}\theta = -2\left(T_1 - T_2\right)/n, \tag{3.194}$$

where $n$ is the average mean motion of either mass. From Kepler's third law $\dot{\theta}/n = -(3/2)s/a$, where $a$ is the average semi-major axis of either mass. Solving the resulting equation for $\mathrm{d}s/\mathrm{d}\theta$ with boundary values $(s_i, \theta_i)$ and $(s_j, \theta_j)$ we obtain

$$\left(\frac{s_i}{a}\right)^2 - \left(\frac{s_j}{a}\right)^2 = \frac{8}{3}\mathcal{G}\frac{m_1 + m_2}{n^2a^3}\int_{\theta_i}^{\theta_j}\bar{H}(\theta)\,\mathrm{d}\theta = -\frac{4}{3}\mathcal{G}\frac{m_1 + m_2}{n^2a^3}\left[H(\theta_i) - H(\theta_j)\right]. \tag{3.195}$$

Note from Eq. (3.191) that $\bar{H}(\theta)$, and hence $T_1$ and $T_2$, are zero at $\theta = \pm 60^\circ$ and therefore the equilibrium configuration is an equilateral triangle of side $r$, with all bodies stationary in a reference frame rotating with mean motion $n$ where

$$n^2r^3 = \mathcal{G}\left(m_c + m_1 + m_2\right). \tag{3.196}$$

However, we have assumed $r \approx a$ and so in order to be consistent we also assume $m_c + m_1 + m_2 \approx m_c$. Therefore we can write Eq. (3.195) as

$$\left(\frac{s_i}{a}\right)^2 - \left(\frac{s_j}{a}\right)^2 = -\frac{4}{3}\frac{m_1 + m_2}{m_c}\left[H(\theta_i) - H(\theta_j)\right]. \tag{3.197}$$

Note that this reduces to Eq. (3.180) in the case when $m_2 \ll m_1$. The equivalence of the two equations shows the generality of the relationship between the orbit and the zero-velocity curve. Similarly, the generalised versions of Eqs. (3.182) and (3.183) are

$$\left(\frac{s}{a}\right)_{\text{crit}} = \left(\frac{8}{3}\right)^{1/2}\left(\frac{m_1 + m_2}{m_c}\right)^{1/2} \tag{3.198}$$

and

$$\left(\frac{s_{180}}{a}\right)^2 = \frac{4}{3}\left(\frac{m_1 + m_2}{m_c}\right)\left[H(\theta_{\min}) - 1\right]. \tag{3.199}$$

Now we are in a position to apply these analytical results to the Janus and Epimetheus system. When the satellites were discovered they had a radial separation of $s_i = \Delta a_0 = 50$ km and an angular separation $\theta_i = 180^\circ$. Substituting these values in Eq. (3.197) with $m_2/m_1 = 0.25$ we can find the variation of $s$ with $\theta$. Writing the semi-major axes of each satellite as $a_J = a + \Delta a_J$ and $a_E = a + \Delta a_E$ we can make use of Eq. (3.184) and the fact that the ratio of the length of each orbital arc is also the ratio of the masses to show the variation of $\Delta a_J$ and $\Delta a_E$ around the orbits in the rotating frame (see Fig. 3.25). Note that the smaller arc or horseshoe is associated with Janus, the larger satellite. As noted above the existence of the triangular equilibrium configuration carries over into the nonrestricted problem. Just as the orbits in the restricted problem had maximum radial width when the test particle had a separation of $\pm 60^\circ$ from the secondary mass (see Figs. 3.18 and 3.20), so in the more general case we see that the radial width of each orbital path is a maximum when the separation of the satellites is $\pm 60^\circ$.

Figure 3.26 shows the paths of the satellites in a frame rotating with the mean motion of either satellite. Here we have exaggerated the radial variation – in reality the half-widths of the Janus and Epimetheus arcs are 10 km and 40 km respectively and each orbit has a mean semi-major axis of 150,432 km. The paths show that the satellites never pass one another. Instead, at four-year intervals their mutual gravitational perturbations cause an exchange of angular momentum: The satellite on the outer path moves to an inner one and vice versa.

Using the theory described above, Dermott & Murray (1981b) showed how observations of the motions of Janus and Epimetheus could be used to determine the sum of the masses as well as their ratio. This can be achieved by making use of Eq. (3.199). Figure 3.27 shows a plot of the minimum angular separation of the two guiding centres as a function of the combined mass of

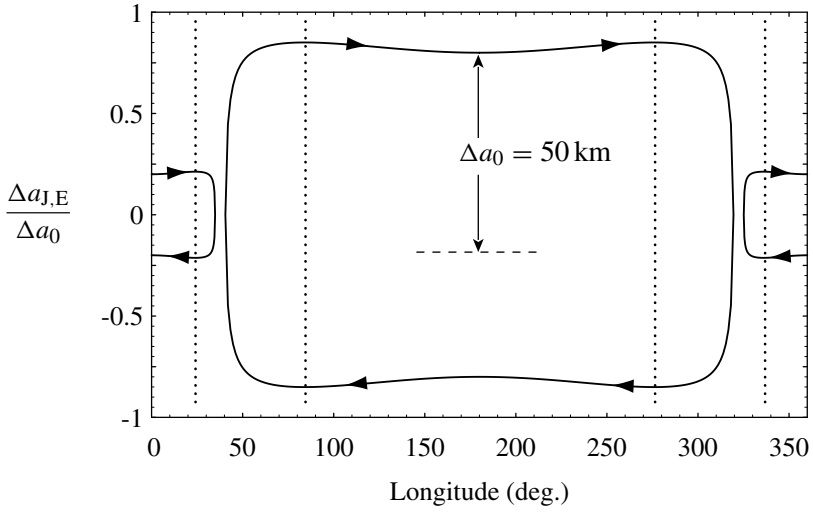


Fig. 3.25. The variation of $\Delta a_J/\Delta_0$ and $\Delta a_E/\Delta a_0$ as a function of longitude in the rotating frame for the Janus–Epimetheus system, where $\Delta_0 = 50$ km is the separation in semi-major axis of the two orbits when the satellites are 180° apart. The dotted lines denote the longitudes of the maximum radial width. Note that these occur when the angular separation of Janus and Epimetheus is ±60°.

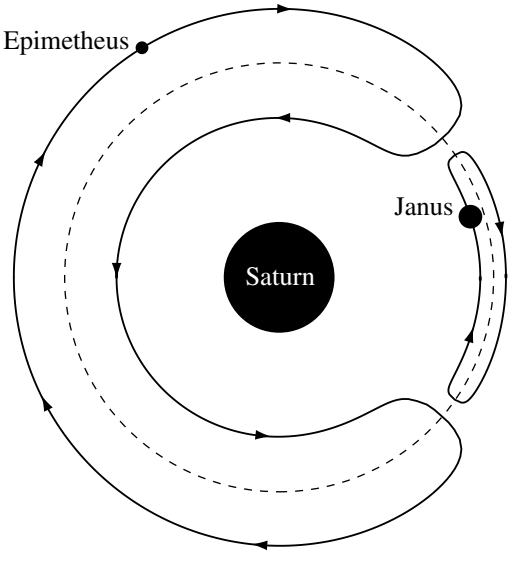


Fig. 3.26. A schematic diagram of the librational behaviour of the Janus and Epimetheus coorbital system in a frame rotating with the average mean motion of either satellite. The radial extent of the librational arcs are exaggerated; the ratio of the radial widths of the arcs is equal to the Janus–Epimetheus mass ratio ($\sim 0.25$).

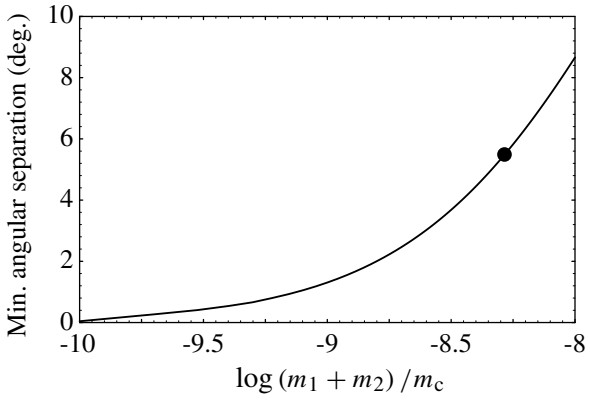


Fig. 3.27. The variation of the minimum angular separation of the two masses as a function of their combined mass. The point denotes the values that have been fitted to the Janus–Epimetheus system.

the satellites, taking $s_{180}/a = 3.32 \times 10^{-4}$. Although this is only an approximation, Dermott & Murray (1981b) showed by numerical integration that the results are accurate to within 0.001°. Nicholson et al. (1992) combined their own ground-based astrometric observations with existing data and derived a new solution for the orbits. This showed that Janus and Epimetheus can approach one another to within 5.64° and that the resulting masses yield densities of $0.65 \pm 0.08$ g cm$^{-3}$ and $0.63 \pm 0.11$ g cm$^{-3}$ respectively. Given that all the evidence from *Voyager* images suggests that these are icy bodies, such low values for the densities points towards the possibility that the small satellites of Saturn may be made of porous ice. This illustrates how knowledge of the dynamics of satellite orbits can lead directly to constraints on their internal properties.

## 3.13 Hill's Equations

For the small particle moving around the central, primary mass in the circular restricted problem the major orbital perturbations will only occur when it encounters the secondary mass. We have already seen examples of such behaviour in the integrations shown in Sect. 3.9; most of the time the particle moves on an unperturbed keplerian orbit. Therefore, instead of dealing with the full equations of the circular restricted three-body problem, it makes more sense to work with a system of equations that describe the motion of the particle in the vicinity of the secondary mass. Such a system was originally derived by Hill (1878) and we will make use of it in the derivation of an encounter map in Sect. 9.5.3 as well as in our study of the shepherding of narrow rings in Sect. 10.5.2.

It is possible to derive such a set of approximate equations by making various assumptions and transferring the origin of the coordinate system to the second mass. For small mass ratios $\mu_1 \approx 1$ and the planar equations of motion, Eqs. (3.16) and (3.17), become

$$\ddot{x} - 2\dot{y} - x = -\frac{x}{r_1^3} - \mu_2 \frac{x-1}{r_2^3}, \tag{3.200}$$

$$\ddot{y} + 2\dot{x} - y = -\frac{y}{r_1^3} - \mu_2 \frac{y}{r_2^3}. \tag{3.201}$$

We now transform the $x$ axis such that $x \to 1 + x$ leaving the $y$ axis unchanged, and let $\Delta = r_2$. Since we are now considering motion close to the satellite (i.e., in the vicinity of the $L_1$ and $L_2$ points) we can assume that $x$, $y$, and $\Delta$ are small quantities of $\mathcal{O}(\mu_2^{1/3})$. Neglecting higher powers of $\mu_2$ we have $r_1 \approx (1 + 2x)^{1/2}$ and Eqs. (3.200) and (3.201) can be written

$$\ddot{x} - 2\dot{y} = \left(3 - \frac{\mu_2}{\Delta^3}\right) x = \frac{\partial U_{\mathrm{H}}}{\partial x}, \tag{3.202}$$

$$\ddot{y} + 2\dot{x} = -\frac{\mu_2}{\Delta^3} y = \frac{\partial U_{\mathrm{H}}}{\partial y}, \tag{3.203}$$

where

$$U_{\mathrm{H}} = \frac{3}{2}x^2 + \frac{\mu_2}{\Delta} \quad \text{and} \quad \Delta^2 = x^2 + y^2, \tag{3.204}$$

and the modified Jacobi constant, $C_{\mathrm{H}}$, is given by

$$C_{\mathrm{H}} = 3x^2 + 2\frac{\mu_2}{\Delta} - \dot{x}^2 - \dot{y}^2. \tag{3.205}$$

We can compare this with the Jacobi constant in the full problem by setting $n = 1$ and ignoring the $z$ motion in Eq. (3.29). This gives

$$C_{\mathrm{J}} = x^2 + y^2 + 2\left(\frac{\mu_1}{r_1} + \frac{\mu_2}{r_2}\right) - \dot{x}^2 - \dot{y}^2. \tag{3.206}$$

Equations (3.202) and (3.203) are called *Hill's equations* and were first derived in connection with Hill's work on lunar theory.

Inspection of Eq. (3.202) reveals that the radial force vanishes when $3\Delta^3 = \mu_2$, expressing the equilibrium between the tidal force and the mutual attraction (cf. Sect. 4.6). This leads to the definition of the *Hill's sphere* as the sphere of radius

$$\Delta_{\mathrm{H}} = \left(\frac{\mu_2}{3}\right)^{\frac{1}{3}} \tag{3.207}$$

surrounding the secondary mass (cf. Eq. (3.75)).

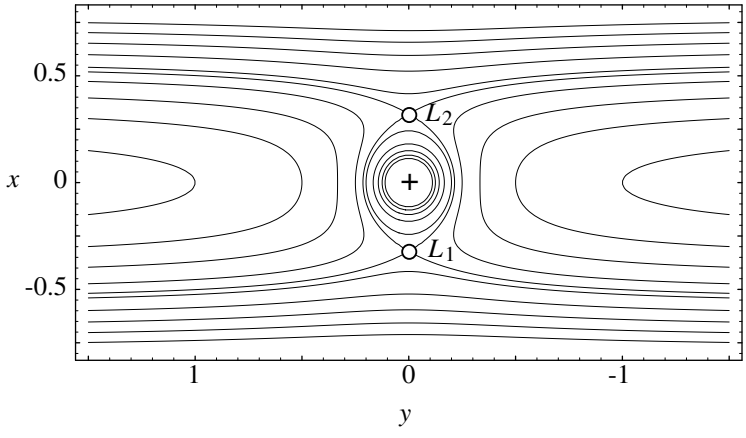


Fig. 3.28. The zero-velocity curves defined by the equation $C_{\rm H} = 2U_{\rm H}$ in the vicinity of the Lagrangian points $L_1$ and $L_2$ for a mass $\mu_2 = 0.1$. Note that in the Hill's approximation the equilibrium points are now equidistant from the mass $\mu_2$ (denoted by the cross at the origin).

By setting $\dot{x} = \dot{y} = \ddot{x} = \ddot{y} = 0$ with $(x \neq 0)$ in Eqs. (3.202) and (3.203) we can find the location of the Lagrangian points $L_1$ and $L_2$. Equation (3.202) gives $\Delta_{L_{1,2}} = (\mu_2/3)^{1/3}$ and Eq. (3.205) gives the corresponding value of the modified Jacobi constant as $C_{\rm H} = 3^{4/3}\mu_2^{2/3}$, in agreement with the values derived for the limiting mass case in Sect. 3.6. Note that the $L_1$ and $L_2$ points lie on the Hill's sphere as we defined it in Eq. (3.207) above. If we write

$$C_{\rm H} = \zeta \mu_2^{2/3} \tag{3.208}$$

then horseshoe motion is possible in the region where $\zeta < 3^{4/3}$. The shapes of the resulting zero-velocity curves in the vicinity of $L_1$ and $L_2$ are shown in Fig. 3.28.

We can use the above definitions to study the relationship between horseshoe orbits and their associated zero-velocity curves in the case where the orbits are near circular. For motion in a circle we have $\dot{x} = \ddot{x} = \ddot{y} = 0$ and $x$ and $\dot{y}$ are constants related by

$$\dot{y}^2 = 3x^2 - \zeta \mu_2^{2/3}, \tag{3.209}$$

where we have used Eqs. (3.205) and (3.208) and assumed that $\Delta$ is large. If $x_{\rm zv}$ denotes the $x$ value (i.e., the half-width) of the zero-velocity curve associated with this horseshoe orbit, then by setting $\dot{y} = 0$ we have

$$x_{\rm zv}^2 = \frac{1}{3}\zeta \mu_2^{2/3}. \tag{3.210}$$

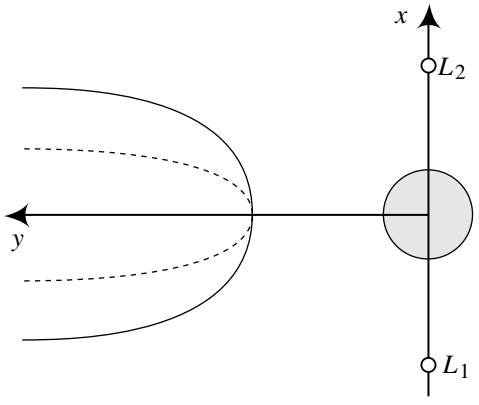


Fig. 3.29. A schematic diagram showing the relationship between a near-circular particle orbit (solid line) and its associated zero-velocity curve (dashed line) using the approximations of Hill's equations.

But $n^2a^3 = 1$ and hence $\dot{y} = -(3/2)x$, giving

$$x^2 = \frac{4}{3}\zeta\mu_2^{2/3}. \tag{3.211}$$

Therefore $x = 2x_{zv}$ and the width of the particle orbit is twice the width of its associated zero-velocity curve, as we already have seen in the case of the full equations (see Sect. 3.10). This is illustrated schematically in Fig. 3.29.

Although these results were derived assuming a near-circular orbit, they are equally applicable in the eccentric case if the orbit is taken to represent the motion of the guiding centre, rather than the particle path. Further details can be found in the work of Dermott & Murray (1981a,b).

We can use Tisserand's criterion to derive a relationship between the orbital elements before and after a satellite encounter using the approximate equations of motion derived above. Let the initial orbital elements be $a_1 = 1+\Delta a_1, e = \Delta e_1$ and the final elements be $a_2 = 1 + \Delta a_2$, $e = \Delta e_2$, where $\Delta a_1$, $\Delta a_2$, $\Delta e_1$, and $\Delta e_2$ are all small quantities. From Sect. 3.4 Tisserand's criterion gives

$$\frac{1}{1+\Delta a} + 2(1+\Delta a)^{1/2}(1-\Delta e^2)^{1/2} \approx \text{constant}, \tag{3.212}$$

which can be expanded binomially to give

$$\frac{3}{4}\Delta a^2 - \Delta e^2 \approx \text{constant} \tag{3.213}$$

or

$$\frac{3}{4}\Delta a_1^2 - \Delta e_1^2 \approx \frac{3}{4}\Delta a_2^2 - \Delta e_2^2. \tag{3.214}$$

Thus, if the orbit is symmetric about the unit semi-major axis (i.e., we have $\Delta a_1 \approx -\Delta a_2$) then $\Delta e_1 \approx \Delta e_2$.

We can also derive the same relationship by considering Hill's equations. If $\Delta$ is large in Eqs. (3.202) and (3.203) we have

$$\ddot{x} - 2\dot{y} = 3x, \tag{3.215}$$

$$\ddot{y} + 2\dot{x} = 0, \tag{3.216}$$

where we can use Eqs. (3.205) and (3.208) to write

$$\dot{x}^2 + \dot{y}^2 = 3x^2 - \zeta \mu_2^{2/3}. \tag{3.217}$$

If we now use the guiding centre approximation, then the radial excursions of the particle are harmonic with frequency $n = 1$ and amplitude equal to the epicyclic eccentricity and we can write $x = \Delta a + e \sin t$, $\dot{x} = e \cos t$, and $\ddot{x} = -e \sin t$. Hence, from Eqs. (3.215) and (3.216) we have $\ddot{y} = -2e \cos t$ and

$$\dot{y} = -\frac{3}{2}\Delta a - 2e \sin t. \tag{3.218}$$

The first term on the right-hand side of Eq. (3.218) represents the (constant) velocity of the guiding centre while the second term represents the varying velocity on the particle's elliptical path about the guiding centre. Using these expressions for $\dot{x}$, $\dot{y}$, and $x$ in Eq. (3.217) we have

$$e^2 \cos^2 t + \left(-\frac{3}{2}\Delta a - 2e \sin t\right)^2 = 3(\Delta a + e \sin t)^2 - \zeta \mu_2^{2/3}, \tag{3.219}$$

from which we can easily derive

$$\frac{3}{4}\Delta a^2 - \Delta e^2 = \zeta \mu_2^{2/3}, \tag{3.220}$$

where the right-hand side is a constant.

The symmetry of the particle's trajectory (or, if the orbit is eccentric, that of its guiding centre) about the $y$ axis allows us to find an expression for its minimum separation, $\Delta_{\min}$, from the secondary mass; this occurs when the particle crosses the $y$ axis (see Fig. 3.29). Consider a particle initially moving on a circular orbit with semi-major axis $1 + \Delta a_0$. In Hill's system the particle's initial position is $(x_0, y_0)$ and Eq. (3.218) gives

$$\dot{y}_0 = -\frac{3}{2}x_0 = -\frac{3}{2}\Delta a_0. \tag{3.221}$$

Hence, from Eq. (3.205),

$$|\Delta a_0| = 2(\zeta/3)^{1/2}\mu_2^{1/3}. \tag{3.222}$$

If we assume that the particle's path is symmetrical about the $y$ axis then at closest approach to the secondary $x = 0$, $\dot{y} = 0$, $\dot{x} = \dot{x}_{\min}$, and $y = \Delta_{\min}$, where

$\dot{x}_{\min}$ is the value of $\dot{x}$ at the crossing point. Equation (3.205) gives

$$\dot{x}_{\min}^2 = 2\frac{\mu_2}{\Delta_{\min}} - \zeta\mu_2^{2/3}. \tag{3.223}$$

In practice $\dot{x}_{\min}^2 \ll \dot{y}_0^2$ (see Dermott & Murray 1981a) and hence

$$y_{\min} \approx (2/\zeta)^{1/2}\mu_2^{1/3} \tag{3.224}$$

or, in terms of $\Delta a_0$,

$$y_{\min} \approx \frac{8}{3}\Delta a_0^2\mu_2. \tag{3.225}$$

Here we have made use of the fact that the guiding centre of the epicyclic path grazes its associated zero-velocity curve when it crosses the $y$ axis. Remember that we have to distinguish between the zero-velocity curve associated with the motion of the guiding centre, which has a fundamental role in determining the particle's trajectory, and the zero-velocity curve associated with the total motion, which, for these purposes, is largely irrelevant.

Another interesting property of Hill's equations is that the system equations scale as $\mu_2^{1/3}$. If we carry out the transformations $x \to x'(\mu_2/3)^{1/3}$, $y \to y'(\mu_2/3)^{1/3}$, $\Delta \to \Delta'(\mu_2/3)^{1/3}$ in Eqs. (3.202) and (3.203) we obtain the equations

$$\ddot{x}' - 2\dot{y}' = \quad 3x'\left(1 - \frac{1}{\Delta'^3}\right), \tag{3.226}$$

$$\ddot{y}' + 2\dot{x}' = -3\frac{y'}{\Delta'^3}. \tag{3.227}$$

These equations contain no parameters, which implies that provided $\mu_2^{1/3} \gg \mu_2$, the particle paths will scale appropriately. In this system of scaled units the $L_1$ and $L_2$ points are at unit distance from the mass $\mu_2$. A selection of librating and circulating trajectories for the scaled equations is shown in Fig. 3.30. All the trajectories in Fig. 3.30 were started on circular orbits at large positive and negative values of $y'$. Note that the particles that were started close to the $y'$ axis ($|x'| < 1.7$) are all "reflected" and move in horseshoe orbits, although those that get close enough to the perturber can achieve a significant eccentricity as a result of the encounter. However, as the initial value of $|x'|$ is increased, there is a zone in which significant perturbations can occur with the result that particles obtain large eccentricities; most pass the perturber but some can still be "reflected" into horseshoe orbits. For the larger values of $|x'|$ the particles pass the perturber and move in circulating orbits. The eccentricity acquired during the encounter becomes negligible as the initial value of $|x'|$ increases. We will consider this type of behaviour in the context of narrow planetary rings in Sect. 10.5.

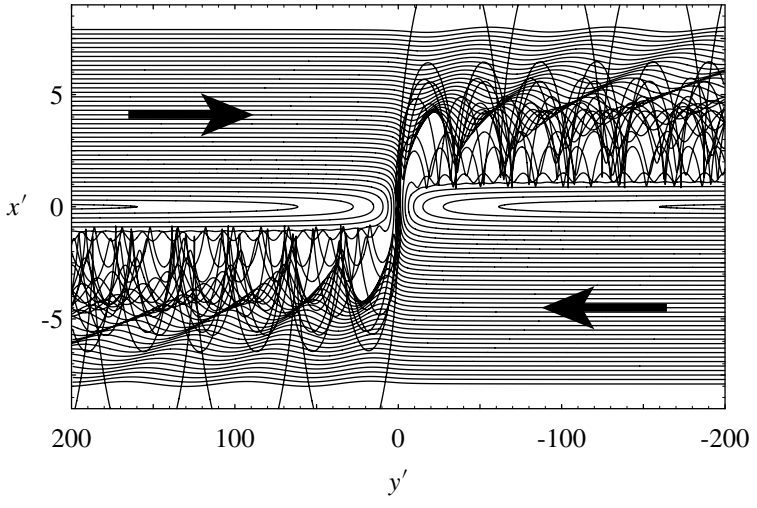


Fig. 3.30. Particle trajectories obtained by solving the scaled form of Hill's equations. The perturbing mass is located at the origin and the $L_1$ and $L_2$ points are at $y' = 0$, $x' = \pm 1$. The particles were all started with $\dot{x}' = 0$ (i.e., in circular orbits) at $y' = \pm 200$. The arrows indicate their direction of motion before encountering the perturber.

## 3.14 The Effects of Drag

The discovery of narrow, sharp-edged rings around Uranus (Elliot et al. 1977) posed a number of severe dynamical problems (see Sect. 10.2.3 and Sect. 10.5.1). One of these concerned the fact that narrow rings should spiral in towards the planet under the effects of Poynting–Robertson (PR) light drag (see Burns et al. (1979) for a comprehensive review of the various radiation forces that can be experienced by small particles in the solar system). PR drag is caused by the nonuniform reemission of the sunlight that a particle absorbs. The particle experiences a drag force, which causes its orbit to decay at a rate dependent on its size, the force being most effective for particles of a size comparable to the wavelength of the incident radiation (i.e., $\sim 10^{-6}$m). In the case where the central mass is the source of the radiation, the PR drag force has the form

$$\mathbf{F} = -\frac{\beta \mathcal{G} m_{\rm c}}{a^2 r^2}\left(\dot{x} - y + \frac{x}{r^2}(x\dot{x} + y\dot{y}),\ \dot{y} + x + \frac{y}{r^2}(x\dot{x} + y\dot{y})\right), \tag{3.228}$$

where $\beta$ is the ratio of the force due to radiation pressure to the gravitational force, $m_{\rm c}$ is the central mass, and $a$ is the semi-major axis of the orbit. Note that the value of $\beta$ depends on such quantities as the luminosity of the source and the radiation pressure cross section. The term involving $\mathbf{r} \cdot \dot{\mathbf{r}}$ in each component of the force in Eq. (3.228) represents the Doppler shift of the incident radiation and the second term is the Poynting–Robertson drag (see Schuerman 1980).

Dermott & Gold (1977) proposed that the narrow rings of Uranus could be explained by the presence in each ring of a small satellite ($\mu_2 < 10^{-10}$) maintaining ring particles in horseshoe orbits. The theory was subsequently extended by Dermott et al. (1980) to the narrow rings of Saturn and Jupiter. PR drag should cause the ring particles to spiral in towards the planet (Burns et al. 1979). However, in the horseshoe orbit model the decay of the particle orbit in one half of the horseshoe would, to a first approximation, be cancelled out by the decay in the other half (Fig. 3.31). The stability of planetary rings are discussed further in Chapter 10.

There are frequent references in the literature to the fact that $L_4$ and $L_5$ are points of potential maximum, and a number of authors have assumed that any dissipation will cause motion away from such points, regardless of the form of the drag force. In fact, as we shall demonstrate, the stability of the triangular equilibrium points under a specific drag force cannot be deduced from simple energy arguments alone. Blitzer (1982) has studied the whole question of stable motion at potential maxima, while Yoder et al. (1983) pointed out the danger of using such arguments in the case of the libration amplitude of the Janus–Epimetheus system.

The particle in the restricted three-body problem can rarely be considered in isolation. In reality, any small particle is subjected to a number of external forces of varying magnitudes in addition to gravitational perturbations. For example, a number of studies have been carried out on the effects of radiation pressure in the three-body problem (see, e.g., Colombo et al. 1966, Schuerman 1980, and

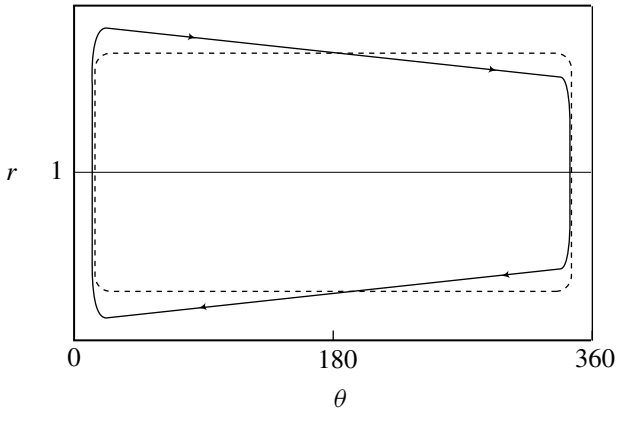


Fig. 3.31. A schematic diagram of the path in the rotating frame (radius $r$ as a function of angle $\theta$) of a particle in a horseshoe orbit subjected to a drag force (solid line) compared with its original path when no drag forces are operating (dashed line). The particle is assumed to have an eccentricity $e \approx 0$. The particle encounters the perturbing mass at $r = 1; \theta \approx 0^\circ, 360^\circ$.

Simmons et al. 1985). Below we consider the dynamical effects of drag forces on the particle using two different approaches: (i) a study of the behaviour of zero-velocity curves and (ii) a study of the location and stability of the Lagrangian equilibrium points. These are the approaches taken by Murray (1994b) in his study of the effects of drag in the circular restricted three-body problem.

In what follows the particle is considered to move under the gravitational attraction of $\mu_1$ and $\mu_2$ and an arbitrary external force, $\mathbf{F} = (F_x, F_y)$, which is a function of the particle's position and velocity. It is assumed that $|\mathbf{F}| = \mathcal{O}(k)$, where $k$ is a small quantity.

### 3.14.1 Analysis of the Jacobi Constant

From Sect. 3.2, the equations of motion of the particle in the rotating frame are

$$\ddot{x} - 2\dot{y} = \frac{\partial U}{\partial x} + F_x, \tag{3.229}$$

$$\ddot{y} + 2\dot{x} = \frac{\partial U}{\partial y} + F_y. \tag{3.230}$$

If we multiply Eq. (3.229) by $\dot{x}$ and Eq. (3.230) by $\dot{y}$ and, then add we get

$$\dot{x}\ddot{x} + \dot{y}\ddot{y} - \left(\dot{x}\frac{\partial U}{\partial x} + \dot{y}\frac{\partial U}{\partial y}\right) = \dot{x}F_x + \dot{y}F_y. \tag{3.231}$$

Because the Jacobi constant in the standard problem can be written as $C_\mathrm{J} = 2U - \dot{x}^2 - \dot{y}^2$ we have

$$\frac{\mathrm{d}C_\mathrm{J}}{\mathrm{d}t} = -2\left(\dot{x}F_x + \dot{y}F_y\right). \tag{3.232}$$

Note that $\dot{x}F_x + \dot{y}F_y$ is the work done by $\mathbf{F}$ per unit time. If we assume that $k < 0$ for a force that opposes the motion, the sign of $\dot{C}_\mathrm{J}$ is opposite to the sign of $\dot{x}F_x + \dot{y}F_y$. From our study of zero-velocity curves in Sect. 3.3 we know that increasing values of $C_\mathrm{J}$ imply increasing areas of exclusion and motion away from the $L_4$ and $L_5$ points. We will consider two illustrative examples.

If the drag force is proportional to the velocity of the particle in the rotating, synodic frame then $\mathbf{F} = k\mathbf{v} = k(\dot{x}, \dot{y})$ and

$$\dot{x}F_x + \dot{y}F_y = k(\dot{x}^2 + \dot{y}^2) < 0. \tag{3.233}$$

Hence this drag force, sometimes called *nebular drag*, causes motion away from the $L_4$ and $L_5$ points, independent of the path of the particle. This result was known to Jeffreys (1929).

In the case of the PR drag component of the radiation force, we have

$$\mathbf{F} = k(\dot{x} - y, \dot{y} + x)/r^2 \tag{3.234}$$

and hence

$$\dot{x}F_x + \dot{y}F_y = k(\dot{x}^2 + \dot{y}^2) - k(\dot{x}y - \dot{y}x). \tag{3.235}$$

However, the sign of this expression cannot be determined by simple inspection – we must know the path of the particle and this cannot be determined for arbitrary starting conditions. Therefore, there are certain drag forces for which this analysis of the Jacobi constant cannot be used to determine stability.

### 3.14.2 Linear Stability of the $L_4$ and $L_5$ Points

We now consider the alternative approach of using a linear stability analysis of the Lagrangian points to establish their local stability behaviour. Here we are concerned with the triangular points since these are the ones that are linearly stable in the zero-drag case. Our approach is based on that by Schuerman (1980), but we follow Murray (1994b) and generalise it to deal with arbitrary drag forces. Murray (1994b) derived expressions for the shift in the five Lagrangian equilibrium points as a function of the drag constant and then showed that, to $\mathcal{O}(\mu_2)$, the characteristic equation for perturbed motion around $L_4$ and $L_5$ can be written as

$$\lambda^4 + a_3\lambda^3 + (1 + a_2)\lambda^2 + a_1\lambda + \left(\frac{27}{4}\mu_2 + a_0\right) = 0, \tag{3.236}$$

where the constants $a_i$ $(i = 0, 1, 2, 3)$ are all $\mathcal{O}(k)$ and are given by

$$a_0 = \frac{9}{4}k_{x,x} + \frac{3}{4}k_{y,y} \mp \frac{3\sqrt{3}}{4}(k_{x,y} + k_{y,x}), \tag{3.237}$$

$$a_1 = \frac{9}{4}k_{x,\dot{x}} + \frac{3}{4}k_{y,\dot{y}} + 2(k_{x,y} - k_{y,x}) \mp \frac{3\sqrt{3}}{4}(k_{x,\dot{y}} + k_{y,\dot{x}}), \tag{3.238}$$

$$a_2 = -k_{x,x} - k_{y,y} + 2(k_{x,\dot{y}} - k_{y,\dot{x}}), \tag{3.239}$$

$$a_3 = -k_{x,\dot{x}} - k_{y,\dot{y}}, \tag{3.240}$$

and where the upper and lower signs in Eqs. (3.237) and (3.238) refer to the $L_4$ and $L_5$ points respectively. These definitions depend on the following partial derivatives:

$$\begin{aligned}
k_{x,x} &= \left[\frac{\partial F_x}{\partial x}\right]_0, \quad k_{y,x} = \left[\frac{\partial F_y}{\partial x}\right]_0, \quad k_{x,\dot{x}} = \left[\frac{\partial F_x}{\partial \dot{x}}\right]_0, \quad k_{y,\dot{x}} = \left[\frac{\partial F_y}{\partial \dot{x}}\right]_0, \\
k_{x,y} &= \left[\frac{\partial F_x}{\partial y}\right]_0, \quad k_{y,y} = \left[\frac{\partial F_y}{\partial y}\right]_0, \quad k_{x,\dot{y}} = \left[\frac{\partial F_x}{\partial \dot{y}}\right]_0, \quad k_{y,\dot{y}} = \left[\frac{\partial F_y}{\partial \dot{y}}\right]_0,
\end{aligned} \tag{3.241}$$

where the subscript 0 denotes evaluation of the partial derivatives at the classical equilibrium positions, $x_0 = 1/2 - \mu_2$, $y_0 = \sqrt{3}/2$, rather than their displaced counterparts. This is because all these quantities are constants of $\mathcal{O}(k)$ and because the displacements are of a similar magnitude and assumed small compared with $x_0$ and $y_0$.

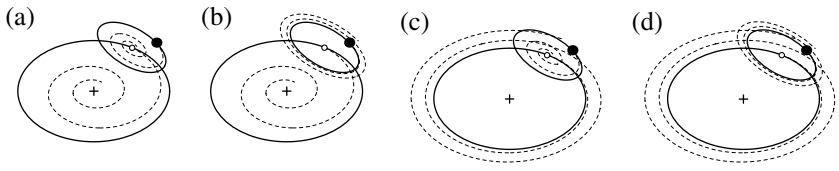


Fig. 3.32. A schematic diagram illustrating the different types of oscillation of the two modes that are possible in the perturbed solution around $L_4$ and $L_5$. The solid lines represent the paths in the absence of drag. The dashed lines show the spiral paths followed in the presence of drag. (a) All real parts of the eigenvalues are negative (asymptotic stability). (b) The real parts of the eigenvalues associated with the motion of the epicentre are negative, but those associated with the epicyclic motion are positive (unstable). (c) The real parts of the eigenvalues associated with the motion of the epicentre are positive, but those associated with the epicyclic motion are negative (unstable). (d) All real parts of the eigenvalues are positive (unstable).

Comparison of Eq. (3.236) with Eq. (3.237) shows that they are equivalent in the case of no drag, because all the $a_i$ are zero and to $\mathcal{O}(\mu_2)$ Eq. (3.236) reduces to the standard bi-quadratic for the classical problem. Without drag the solutions of the characteristic equation are purely imaginary provided that the usual condition on the mass ratio, Eq. (3.145), is satisfied. The situation is more complicated in the presence of drag. Four possibilities arise and each is illustrated in Fig. 3.32.

1) All real parts of the eigenvalues are negative. This gives asymptotic stability.
2) The real parts of the eigenvalues associated with the long-period motion of the epicentre are negative, but those associated with the short-period motion are positive. This is linearly unstable.
3) The real parts of the eigenvalues associated with the long-period motion of the epicentre are positive, but those associated with the short-period motion are negative. This is linearly unstable.
4) All real parts of the eigenvalues are positive. This is linearly unstable.

Note that although one of the eigenmodes may be damped (as in cases 2 and 3 of this list) this does not produce stability since the other mode is exponentially increasing. Murray (1994b) showed that the conditions for each of the real parts of $\lambda$ to be negative, and hence for the points to be asymptotically stable in the limit as $\mu_2 \to 0$, reduce to

$$0 < a_1 < a_3, \tag{3.242}$$

where $a_1$ and $a_3$ are defined in Eqs. (3.238) and (3.240). Note that, with these approximations, the stability is independent of the values of $a_0$ and $a_2$ and thus the linear stability of $L_4$ and $L_5$ does not depend on the values of $k_{x,x}$ and $k_{y,y}$. We can now consider the two drag forces studied above from the point of view of the linear stability of the $L_4$ and $L_5$ points.

If $\mathbf{F} = k(\dot{x}, \dot{y})$ then the only nonzero values of the constants in Eq. (3.241) are

$$k_{x,\dot{x}} = k, \qquad k_{y,\dot{y}} = k, \tag{3.243}$$

and hence

$$a_1 = 3k, \qquad a_3 = -2k. \tag{3.244}$$

Since $k < 0$ we have $a_1 < 0$, the condition in Eq. (3.242) is not satisfied, and the triangular equilibrium points are unstable under this drag force, as we deduced from our study of the Jacobi constant.

In the case of PR drag $\mathbf{F} = k(\dot{x} - y, \dot{y} + x)/r^2$ and the only relevant nonzero values of the constants in Eq. (3.241) are

$$k_{x,\dot{x}} = k_{y,x} = k_{y,\dot{y}} = k, \quad k_{x,y} = -k, \tag{3.245}$$

and hence

$$a_1 = -5k, \qquad a_3 = -2k. \tag{3.246}$$

Therefore the points are linearly unstable to PR drag.

However, it is interesting to note that if we consider a force $\mathbf{F} = k(\dot{x} - y, \dot{y} + x)$ then the only relevant nonzero values of the constants in Eq. (3.241) are

$$k_{x,\dot{x}} = k_{y,x} = k_{y,\dot{y}} = k, \quad k_{x,y} = -k, \tag{3.247}$$

and hence

$$a_1 = -k, \qquad a_3 = -2k. \tag{3.248}$$

In this case the condition in Eq. (3.242) is satisfied and the triangular equilibrium points are asymptotically stable under this drag force. Of course, this gives us no information on the stability of large-amplitude tadpole or horseshoe orbits about these points since our analysis always assumes a small displacement from the equilibrium point.

### *3.14.3 Inertial Drag Forces*

Murray (1994b) considered a general drag force per unit mass of the form

$$\mathbf{F}_{\mathrm{i}} = k\mathbf{V}g(x, y, \dot{x}, \dot{y}), \tag{3.249}$$

where $k < 0$, $\mathbf{V} = (\dot{x} - y, \dot{y} + x)$ is the particle's velocity in the inertial frame, and $g(x, y, \dot{x}, \dot{y})$ is a scalar function of its position and velocity; Murray (1994b) referred to this as an *inertial drag*. Eliminating the drag constant, $k$, from the equations of motion gives

$$r^2 r_1^3 r_2^3 + \mu_2 r_1^3(\mu_1 x - r^2) - \mu_1 r_2^3(\mu_2 x + r^2) = 0 \tag{3.250}$$

for the paths along which the five equilibrium points must move. Figure 3.33a shows these paths for the case $\mu_2 = 0.2$.

In the limit as $\mu_2 \to 0$ Murray showed that $L_3$, $L_4$, and $L_5$ move along the unit circle whereas $L_1$ and $L_2$ move along circles close to the secondary. In cases where $g^* = g(x, y, 0, 0) = g^*(r)$, a function of the radius only, the angular position of $L_4$ and $L_5$ for small $\mu_2$ can be derived from a plot of

$$\frac{\bar{k}}{\mu_2} = \sin\theta \left( \frac{1}{(2 - 2\cos\theta)^{3/2}} - 1 \right), \tag{3.251}$$

where $\bar{k} = kg^*(1)$. This function is shown in Fig. 3.33b. It has a minimum at $\theta = 108.4^\circ$ for $\bar{k}/\mu_2 = -0.7265$ and a maximum at $\theta = 251.6^\circ$ for $\bar{k}/\mu_2 = +0.7265$. Therefore the $L_3$ and $L_4$ points can shift from position angles of $180^\circ$ and $60^\circ$ respectively to a position angle of $108.4^\circ$ for $\bar{k}/\mu_2 = -0.7265$ before disappearing for all values of $\bar{k}/\mu_2 < -0.7265$. This behaviour is independent of the form of $g_r$. In all systems where $g^*$ is a function of $r$ these results show that there are regimes where $L_5$ can survive even though $L_4$ has ceased to exist.

The stability of the shifted $L_4$ and $L_5$ points under inertial drag can be considered using techniques derived in Sect. 3.15.2. For example, Murray (1994b) considered an inertial drag force of the form

$$\mathbf{F}_\mathrm{i} = k\mathbf{V}V^i r^j, \tag{3.252}$$

where $i$ and $j$ are real numbers. He showed that the triangular equilibrium points will be asymptotically stable to this drag force provided $k < 0$ and the conditions

$$0 < 1 - i + 2j < 2 + i \tag{3.253}$$

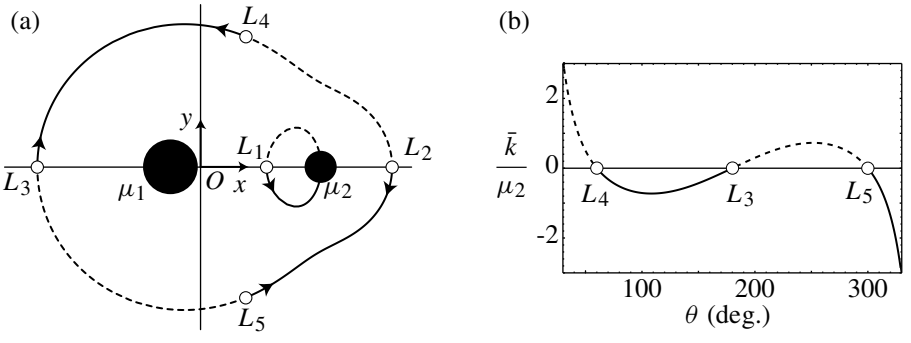


Fig. 3.33. (a) The paths of the shifted Lagrangian equilibrium points in the presence of a general inertial drag force of the form given in Eq. (3.249) for $\mu_2 = 0.2$. (b) The relationship between $\bar{k}/\mu_2$ (where $\bar{k}$ is the modified drag constant defined in the text) and the shifted position angle, $\theta$ (between $30^\circ$ and $330^\circ$) of the $L_3$, $L_4$, and $L_5$ equilibrium points in the case of small mass ratio for an inertial drag. In each diagram the solid lines denote the case when $k < 0$ and the dashed lines the case when $k > 0$. (Adapted from Murray 1994b.)

are satisfied. If we consider the specific case $i = 0$, $j = n$ then this drag force will produce asymptotic stability in $L_4$ and $L_5$ provided $-1/2 < n < 1/2$. This highlights the need to consider each drag force separately when discussing the stability of the triangular equilibrium points. Murray (1994b) also showed that in cases where the drag force is large it is possible for the $L_4$ and $L_5$ points to both be unstable but with different $e$-folding timescales. He suggested that this could explain possible asymmetries in the distribution of the Trojan asteroids. The existence of the maximum shifted longitude of $L_4$ at $\theta = 108.4^\circ$ had been observed in numerical experiments by Peale (1993b).

## Exercise Questions

**3.1** Using the standard system of units for the planar, circular, restricted three-body problem, the equation defining the zero-velocity curves is $C_\mathrm{J} = x^2 + y^2 + 2(\mu_1/r_1 + \mu_2/r_2)$, where $C_\mathrm{J}$ is the value of the Jacobi constant and $r_1 = \sqrt{(x+\mu_2)^2 + y^2}$ and $r_2 = \sqrt{(x-\mu_1)^2 + y^2}$ are the distances to the masses $\mu_1$ and $\mu_2$, respectively. The critical zero-velocity curve that passes through the $L_3$ equilibrium point (where $C_\mathrm{J} \approx 3 + \mu_2$) has two branches. Use polar coordinates to show that for small mass ratios each of the curves crosses the unit semi-major axis at points with an angular separation of $23.5^\circ$ from the secondary mass.

**3.2** In the circular restricted three-body problem the condition for the three collinear Lagrangian equilibrium points to be linearly unstable is $\bar{A} > 1$, where $\bar{A} = \mu_1/r_1^3 + \mu_2/r_2^3$ and $r_1$ and $r_2$ (both positive quantities) are the distances to the masses $\mu_1$ and $\mu_2$. Taking $\alpha = ((1/3)\mu_2/\mu_1)^{1/3}$ and $\beta = -(7/12)\mu_2/\mu_1$, where $\mu_2 \ll \mu_1$, derive expressions for $\bar{A}$ including terms up to $\mathcal{O}(\alpha, \beta)$ and show that the condition $\bar{A} > 1$ is satisfied for (i) $L_1$, where $r_1 \approx 1 - \alpha$, $r_2 \approx \alpha$, (ii) $L_2$, where $r_1 \approx 1 + \alpha$, $r_2 \approx \alpha$, and (iii) $L_3$, where $r_1 \approx 1 + \beta$, $r_2 \approx 2 + \beta$. In the case of the $L_3$ point show that the real roots of the characteristic equation, and hence the eigenvalues that give rise to the instability, are approximately $\pm\sqrt{(21/8)\mu_2}$.

**3.3** The centre of mass of a spacecraft is moved to within 1 m of the inner ($L_1$) Lagrangian equilibrium point of Io, one of the moons of Jupiter. Assuming that an analytical solution based on a linear stability analysis is always valid, use the data in Appendix A to calculate how long it would be before the spacecraft hits the surface of Io.

**3.4** Two planetary satellites of masses $m_1$ and $m_2$, semi-major axes $a_1$ and $a_2$, and eccentricities $e_1$ and $e_2$ orbit a planet of mass $m_\mathrm{p}$ (where $m_\mathrm{p} \gg m_1, m_2$) such that at the same time interval before and after their closest approach their semi-major axes are $a_1 = a_0 \pm \Delta a_1$ and $a_2 = a_0 \mp \Delta a_2$, where $a_0$ is the mean semi-major axis of both satellites; their eccentricities are unchanged by the encounter.

Derive expressions for the total orbital angular momentum of the system before and after closest approach by carrying out expansions to second order in $\Delta a_1/a_0$, $\Delta a_2/a_0$, $e_1$, and $e_2$. If the total orbital angular momentum is preserved, use your expressions to show that $\Delta a_1/\Delta a_2 \approx m_2/m_1$.

**3.5** The parameterless form of Hill's equations for the motion of a test particle in the vicinity of the secondary mass are $\ddot{x} - 2\dot{y} = 3x\left(1 - 1/\Delta^3\right)$, $\ddot{y} + 2\dot{x} = -3y/\Delta^3$, where $\Delta = \sqrt{x^2 + y^2}$ is the distance from the secondary. In this system of units the $L_1$ and $L_2$ points are at $y = 0$, $x = \mp 1$. Write a computer program to solve the equations of motion numerically, taking initial values of $x_0$ at intervals of 0.01 between 0.01 and 5 with $y_0 = 200$, $\dot{x}_0 = 0$, and $\dot{y}_0 = -(3/2)x_0$ in all cases. Use your results to find (i) the smallest value of $x_0$ below which the test particle is always "reflected" by the secondary mass, (ii) the smallest value of $x_0$ above which the particle always passes the secondary mass, and (iii) the value of $x_0$ that gives the largest value of $|x|$. How would you characterise the trajectories for values of $x_0$ given in your answers to parts (i) and (ii).

**3.6** The test particle in the circular restricted three-body problem experiences a drag force $\mathbf{F} = k\mathbf{v}v^i r^j$, where $k < 0$ is a constant, $i$ and $j$ are real numbers, and $\mathbf{r} = (x, y)$, and $\mathbf{v} = (\dot{x} - y, \dot{y} + x)$ are the position and velocity vectors (both in the rotating frame) with magnitudes $r$ and $v$. Use the method given in Sect. 3.15.2 to show that for small values of $k$ this drag force results in asymptotic, linear stability of the $L_4$ and $L_5$ equilibrium points provided $0 < 1 - i + 2j < 2 + i$.